Copyright Warning & Restrictions

The copyright law of the United States (Title 17, United States Code) governs the making of photocopies or other reproductions of copyrighted material.

Under certain conditions specified in the law, libraries and archives are authorized to furnish a photocopy or other reproduction. One of these specified conditions is that the photocopy or reproduction is not to be "used for any purpose other than private study, scholarship, or research." If a, user makes a request for, or later uses, a photocopy or reproduction for purposes in excess of "fair use" that user may be liable for copyright infringement,

This institution reserves the right to refuse to accept a copying order if, in its judgment, fulfillment of the order would involve violation of copyright law.

Please Note: The author retains the copyright while the New Jersey Institute of Technology reserves the right to distribute this thesis or dissertation

Printing note: If you do not wish to print this page, then select "Pages from: first page # to: last page #" on the print dialog screen

ABSTRACT

INVESTIGATING NEURAL MECHANISMS OF HAND MOVEMENTS IN VIRTUAL REALITY

by
Chuang Mu

Mirror visual feedback (MVF), a technique by which movement of one limb is perceived as movement of the contralateral limb, has the capacity to relieve phantom limb pain or promote motor recovery of the upper limbs after stroke (Ramachandran et al., 1995). Functional MRI studies have demonstrated activation of the motor areas in the hemisphere ipsilateral to the moving hand in response to MVF. However, the neural mechanisms of MVF are still unclear. This Electroencephalography (EEG) study was designed to investigate the timing of neural responses to MVF presented in virtual reality. 16 right-handed, neurologically healthy subjects participated in a series of four experimental sessions. Two factors (visual feedback: no-mirror (M^-) and mirror (M^+) and movement target: no-goal (G^-) and goal (G^+)) were systematically manipulated to form four testing conditions (M^-G^-, M^+G^-, M^-G^+ and M^+G^+). The time course of cortical oscillations was captured using a 64-channel EEG system (ANT Neuro). Index finger kinematics and surface Electromyogram (EMG) of the right First Dorsal Interosseous (FDI) muscle were synchronized with the EEG signals to explore the timing of MVF effects on cortical activity. In all four conditions, pronounced decrease in power of beta-band activity relative to reference was observed during movement planning and execution in C3 and C4 electrodes (bilateral primary motor cortex). Moreover, MVF reduced inter-hemispheric differences in beta-band power during movement preparation and execution. Significantly stronger reduction in inter-hemispheric power difference

during the execution phase of the movement was observed in the $M^{+}G^{+}$ compared to $M^{+}G^{-}$. In all four conditions, prominent decrease in alpha range power was observed in the P3 and P4 electrodes (bilateral parietal cortex) during the preparation phase. The effect of MVF decreased the asymmetry in hemispheric activation in alpha-range power during the preparation phase of goal-directed movements, $M^{+}G^{+}$ and $M^{-}G^{+}$, when compared to $M^{+}G^{-}$ and $M^{-}G^{-}$ conditions. In addition to spatial- and frequency-specific power analysis, the effects of MVF were also explored using topographic maps which reflect scalp potential distribution. Global field power during movement preparation phase in the $M^{+}G^{+}$ condition was more lateralized to the hemisphere ipsilateral to the moving hand when compared to $M^{-}G^{+}$ condition. In conclusion, MVF applied during unilateral hand movement significantly attenuates hemispheric activation asymmetry.

INVESTIGATING NEURAL MECHANISMS OF HAND MOVEMENTS IN VIRTUAL REALITY

by
Chuang Mu

A Thesis
Submitted to the Faculty of
New Jersey Institute of Technology
and Rutgers, The State University of New Jersey - Newark
in Partial Fulfillment of the Requirements for the Degree of
Master of Science in Biomedical Engineering

Department of Biomedical Engineering

January 2016

APPROVAL PAGE

INVESTIGATING NEURAL MECHANISMS OF HAND MOVEMENTS IN VIRTUAL REALITY

Chuang Mu

Dr. Sergei Adamovich, Dissertation Advisor — Date
Associate Professor of Biomedical Engineering, NJIT

Dr. Richard Foulds, Committee Member — Date
Associate Professor of Biomedical Engineering, NJIT

Dr. Mesut Sahin, Committee Member — Date
Professor of Biomedical Engineering, NJIT

BIOGRAPHICAL SKETCH

Author: Chuang Mu

Degree: Master of Science

Date: January 2016

Undergraduate and Graduate Education:

- Master of Science in Biomedical Engineering,
  New Jersey Institute of Technology, Newark, NJ, 2016

- Bachelor of Biomedical Engineering,
  Changchun University of Science and Technology, Changchun, China, 2009.

Major: Biomedical Engineering

I dedicate this to my mother and father. I am grateful for their encouragement.

ACKNOWLEDGMENT

I would like to thank my thesis advisor, Dr. Sergei Adamovich for his support in the completion of this study. Special thanks to Dr. Mesut Sahin and Dr. Richard Foulds for serving as committee members for this thesis. I am also grateful to the former University of Medicine and Dentistry of New Jersey for their support during data collection and analysis. Finally, the author offers his gratitude to Maryam Rohafza, Mathew Yarossi and Qinyin Qiu from the Neuro Rehabilitation laboratory at NJIT for their support and friendship.

TABLE OF CONTENTS

TABLE OF CONTENTS
(Continued)

Chapter **Page**

LIST OF TABLES

LIST OF FIGURES

LIST OF FIGURES
(Continued)

LIST OF FIGURES
(Continued)

Figure **Page**

LIST OF DEFINITIONS

Kinematic	The analysis of angles and motion of bodies
EEG	Electroencephalography
EMG	Electromyography
ERD	Event-related desynchronization
FDI	First Dorsal Interosseous
MVF	Mirror visual feedback
RMS	Root mean square
ICA	Independent component analysis
SSE	Error sum of squares

CHAPTER 1

INTRODUCTION

1.1 Mirror Visual Feedback (MVF)

Mirror Visual Feedback (MVF) is a technique by which the movement of one limb is perceived as movement of the contralateral limb. MVF is always considered as visual stimulus. Mirror Therapy (MT) was developed based on the MVF which combined movement execution and movement observation together. In 1995, MT was first tested on a patient who lost his left arm by Ramachandran and his team. They found MT can relieve the phantom limb pain after several trainings [1]. Then, MT has received great interest from healthy professionals and much subsequent studies were inspired by this significant finding. These studies used 'mirror box' and Virtual Reality (VR) technique to explore the mechanisms of Mirror Visual Feedback (MVF) or to replicate the Mirror Therapy (MT).

The traditional 'mirror box' consisted of a plain mirror which was vertically placed in the midsagittal plane inside a rectangular box [2]. In the mirror view condition, the subject was instructed to move his while looking at the reflection of the moving hand through the mirror, superimposed on the resting hand. Figure 1.1 showed the traditional 'mirror box'. But the traditional 'mirror box' has disadvantages. It is not convenient to design the very specific goal-oriented motor task. But this shortcoming can be overcome by the novel Virtual Reality (VR) technique because it provides the ability to manipulate the feedbacks. In addition, this technique can also increase the subjects' feeling of engagement, thus encouraging them to repeat the exercise with high intensity. In Figure

1.2, the subject wore the CyberGlove on his left hand, which can simulate the finger motion, to reach goals in a virtual environment but getting the visual feedback from right (mirror) side [3]. In this regard, VR technique has tremendous potential as a tool to for stroke rehabilitation and to explore the effects of MVF.

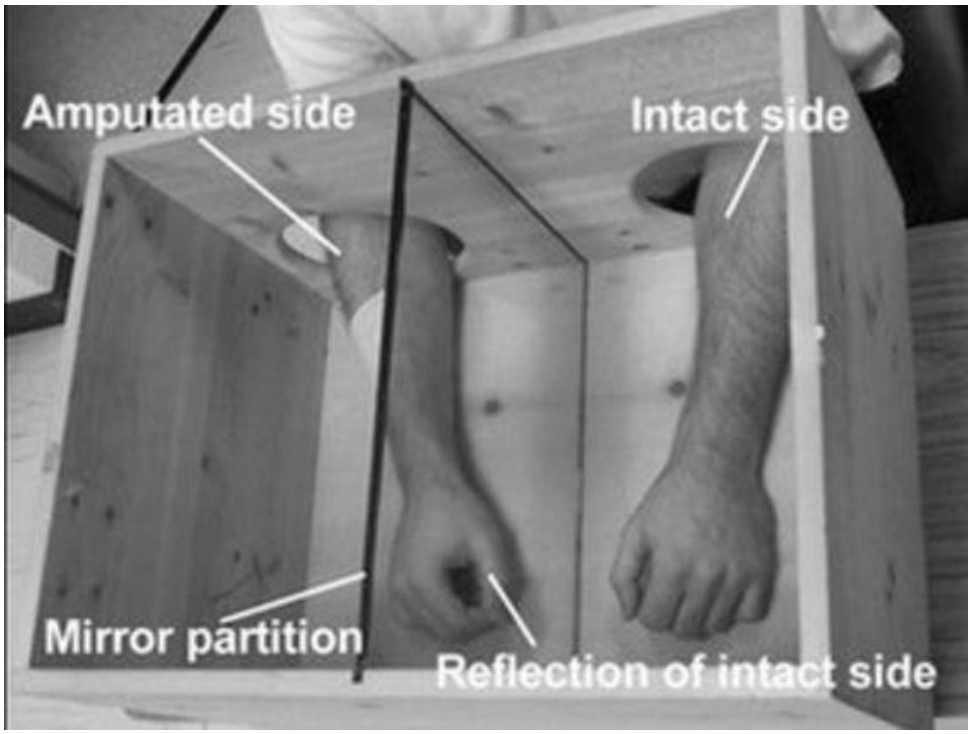

Figure 1.1 Mirror Box. The mirror was placed in the midsagittal plane. The phantom hand was placed behind the mirror. When the patient looked into the mirror he can feel the reflection of the real hand superimposed on the phantom.

Source: http://www.bbc.com/news/magazine-15938103

Figure 1.2 Virtual Reality (VR) system. The subject wore the CyberGlove at his left to control his right (mirror) hand to reach goals under the virtual environment.

Source: Sato, Kenji, et al. "Nonimmersive Virtual Reality Mirror Visual Feedback Therapy and Its Application for the Treatment of Complex Regional Pain Syndrome: An Open Label Pilot Study." Pain medicine 11.4 (2010): 622-629.

The following studies about investigating the effects of MVF using functional MRI, transcranial magnetic stimulation (TMS) and MEG, etc. have confirmed that MVF has the capacity to improve motor functions and to increase the activation over the damaged hemisphere in stroke patients. In detail, these studies revealed that MVF can instantly increase neuronal activation or motor functions over the motor cortex or parietal cortex ipsi- or contralateral to moving hand in patients with stroke [4, 5, and 6]. However, the exact neural mechanism underlying the beneficial effects of MVF remains unclear.

1.2 Electroencephalography (EEG)

The functional MRI was always used to investigate MVF effects because it can mainly focus on finding the areas of brain that response to the MVF stimulus. However, it cannot provide any information about the continuous cortical activity. The time-course study of cortical activation by MVF is critical to determine when and how brain responds to MVF stimulus. In view of this, Electroencephalography (EEG) technique is a powerful tool to investigate the time-course brain activity because it has a high temporal resolution and non-invasive [7]. EEG records the brain electrical changes through electrodes which are always placed on the head. In detail, clusters of neurons will be activated by events and then leading to ionic current changes. These tiny changes get together to lead to electrical changes over the whole brain or specific regions. EEG signal is commonly recorded at sampling rates between 250 and 2000 Hz in clinical and research settings, but advanced EEG data collection systems are capable of recording at sampling rates above 20,000 Hz if desired [8]. In brief, EEG refers to record the brain's spontaneous electrical activity over a phase of time, from multiple electrodes placed on the scalp (Figure 1.3) [9].

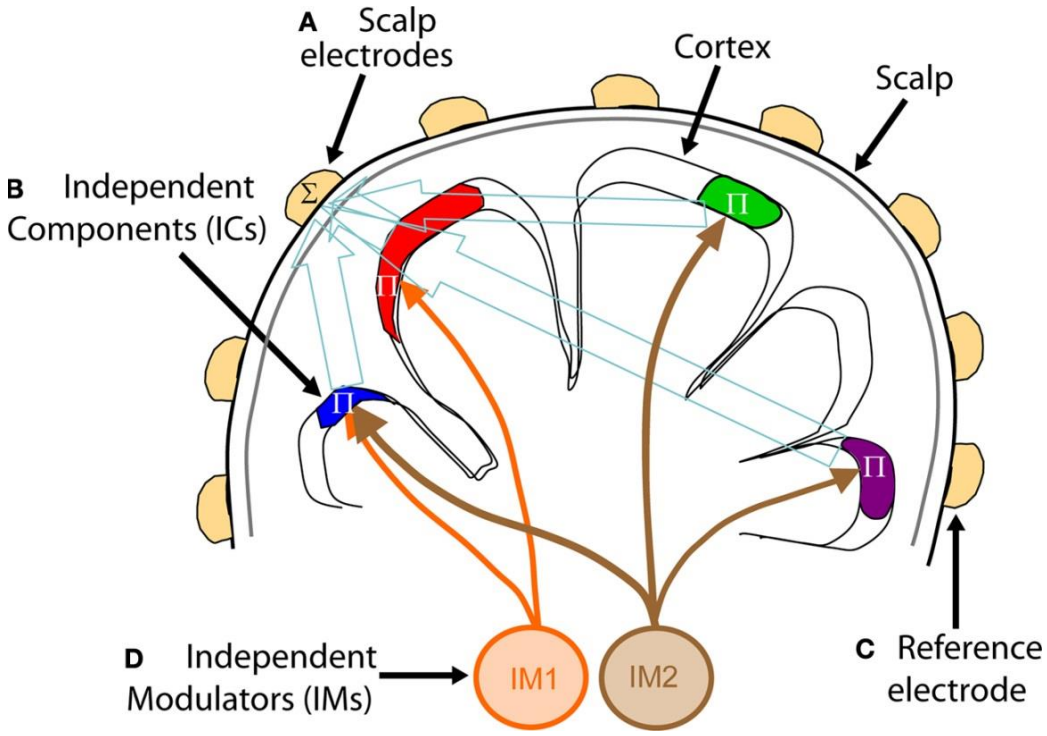

Figure 1.3 Independent spectral modulators of scalp EEG signals. (A) temporally distinct signals generated by partial synchronization of local field potentials within cortical patches or independent components (B), the resulting far-field potentials summed (Σ), in differing linear combinations, at each electrode depending on the distance and orientation of each cortical patch generator relative to the (A) recording and (C) reference electrodes.

Source: http://journal.frontiersin.org/article/10.3389/neuro.09.061.2009/full

1.3 Event-related Synchronization and Desynchronization (ERS/ERD)

Some previous studies about EEG signals revealed that events can induce time-locked changes in the activity of neuronal populations that called event-related potentials (ERPs). In order to explore the ERPs, averaging-trials method is always used. However, some changes of event-induced activity can only be detected in specific frequency bands instead of the broad band ERPs [10]. In addition, previous studies also found that the EEG oscillations can be divided into different frequency bands (Figure 1.4) and each band has its own function [11]. Beta band (12 to 30 Hz) is always associated with movement execution; alpha band (8 to 12 Hz) is related to the processing of sensory-

semantic information and attention. In addition, Beta range power is lowest during movement execution and during changes in isometric muscle contraction. This change is proposed to reflect cortical activity related to upper-limb movements [12]. Alpha range power decreased during goal-directed movements. This activity is presumed to reflect cortical activity related to movement planning and information processing [13]. Researchers confirmed that these power changes, involving increases or decreases, in specific bands reflect the interruption of ongoing oscillatory activity by functionally active neuronal populations [10]. The amplitude decreases in specific frequency-band power called as event-related desynchronization (ERD), and the amplitude increases are referred to as event-related synchronization (ERS) [14]. The phenomenon of power increases (event-related synchronization ERS) or power decreases (event-related desynchronization ERD) of the EEG signals was believed to reflect the basic neurophysiological processes, such as the power decrease reflect the neurons are partially desynchronized at local field by certain events [10]. Now, it is generally accepted that ERS\ERD during the performance of a motor task can work as a reliable marker of excitation neural network because neuronal networks can display different states of synchrony with oscillations at different frequencies [15]. In addition, previous studies proved that specific EEG bands come from different cortical regions [17]. For example, alpha band located at posterior regions of brain on both sides, higher in amplitude on dominant side. Therefore, the measurement of the alpha- and beta-rhythm ERD is an ideal method for exploring the time-course changes in brain.

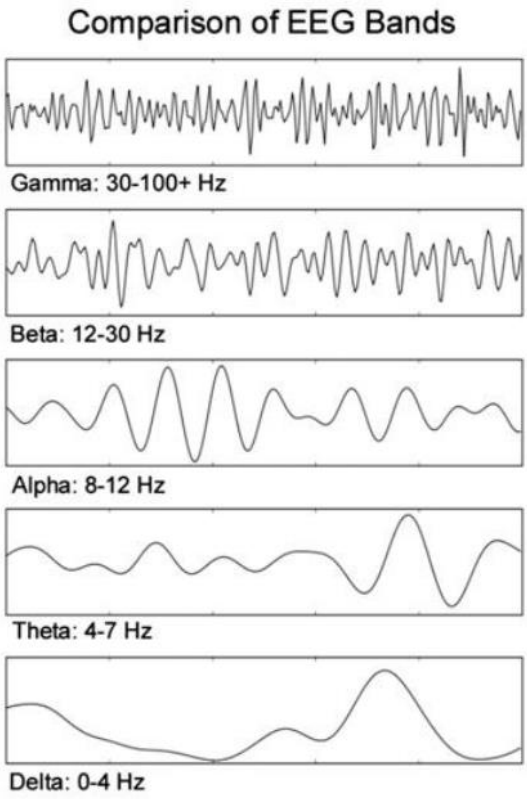

Figure 1.4 Comparison of EEG bands. Top to bottom: Gamma band (> 30Hz); Beta band (12 - 30Hz); Alpha band (8 - 12Hz); Theta band (4 - 7 Hz); Delta band (< 4Hz).

Source: http://neurosky.com/2015/05/greek-alphabet-soup-making-sense-of-eeg-bands/

1.4 Spatial Domain

Another important problem is to investigate the distribution of these EEG frequency oscillations over the scalp. The contralateral motor (M1) and primary somatosensory (S1) regions are shown in the Figure 1.5. This figure illustrates the physical representation of the hand on the motor cortex. One previous study suggested that beta power reduction occurred during hand movements which can be observed from motor cortex [13]. Moreover, during hand movements, in addition to the motor cortex, other cortical regions are also involved (Figure 1.6), such as posterior parietal cortex (PPC). The information traveled from the posterior parietal cortex (PPC) to the supplementary motor area, and

then got together in motor cortex and primary somatosensory cortex. The alpha band ERD was detected from posterior parietal cortex during goal-directed movements [12].

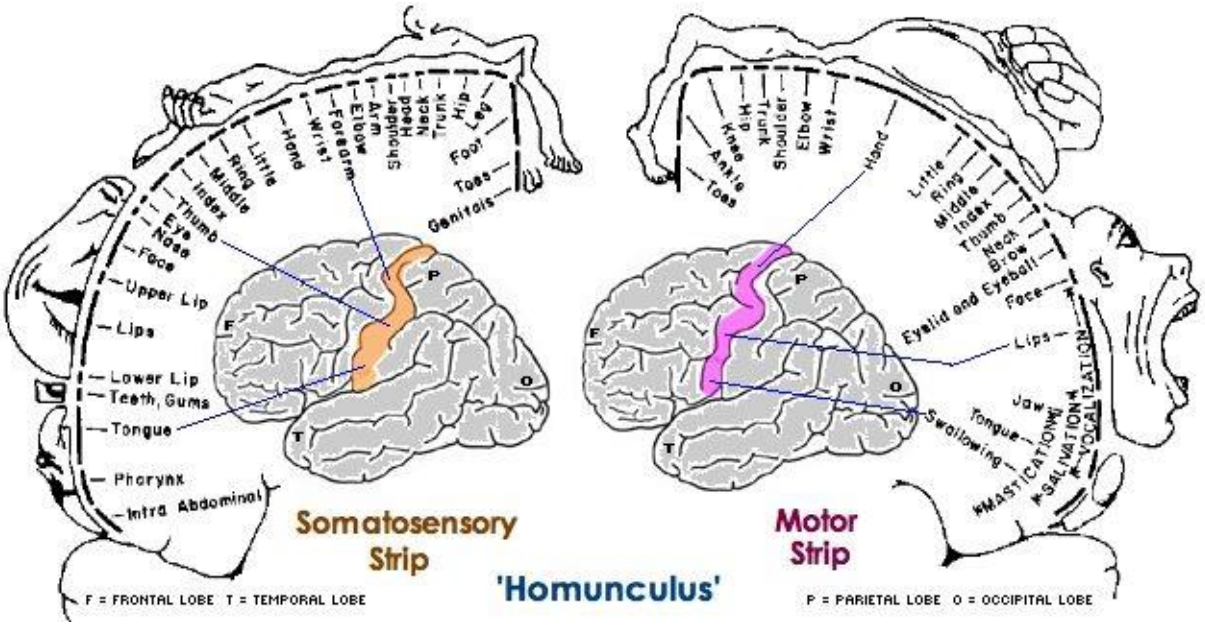

Figure 1.5 Representation of Homunculus on the Motor and Somatosensory regions.

Source: https://www.pinterest.com/pin/446349013042742590/

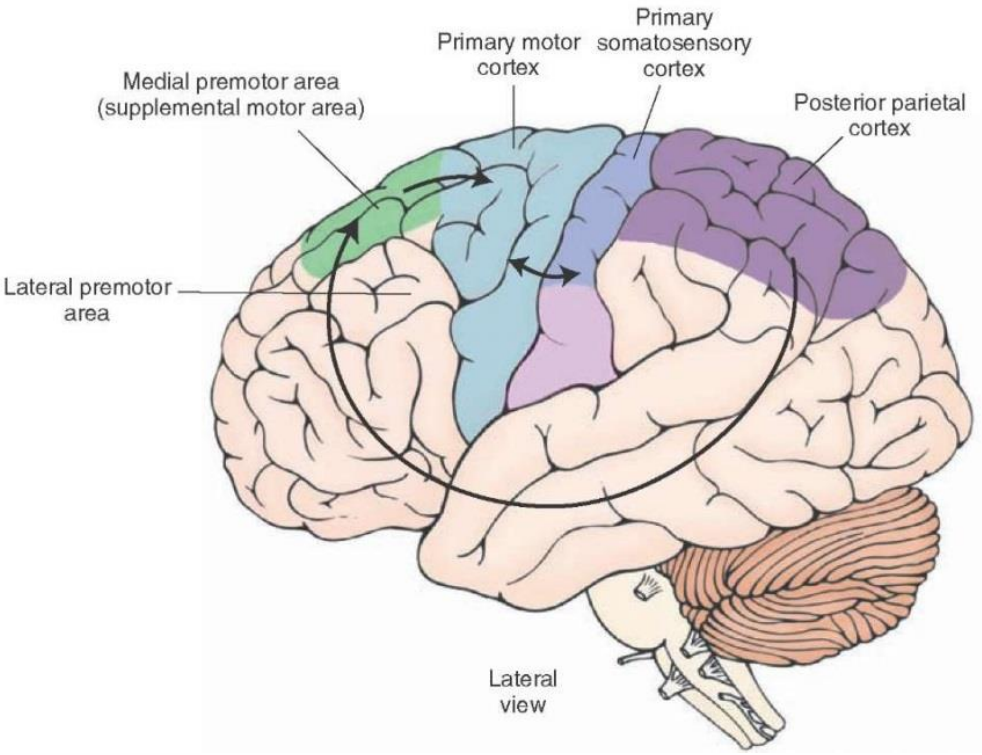

Figure 1.6 Information flow during voluntary movement. The information traveled from the posterior parietal cortex (PPC) to the pre-motor and supplementary motor area (SMA), finally the information worked together in motor cortex and primary somatosensory cortex.

Source:
http://humanphysiology.academy/Neurosciences%202015/BS%20Tutorials/T.4%20Motor%20Pathways.html

1.5 Objective

In this study, neurophysiological effects of mirror visual feedback (MVF) were investigated during right hand movements. During right hand movements, the motor cortex contralateral to moving hand is active. Because motor observation shares the same neural mechanism as motor execution, the visual feedback from the same side of the moving hand would activate the same cortical region. However, if the visual feedback comes from the mirror side of the moving hand, the hemisphere ipsilateral to the moving

hand will be active (Figure 1.7). Thus the first hypothesis is that the asymmetry in hemispheric activation will be reduced by mirror visual feedback (MVF).

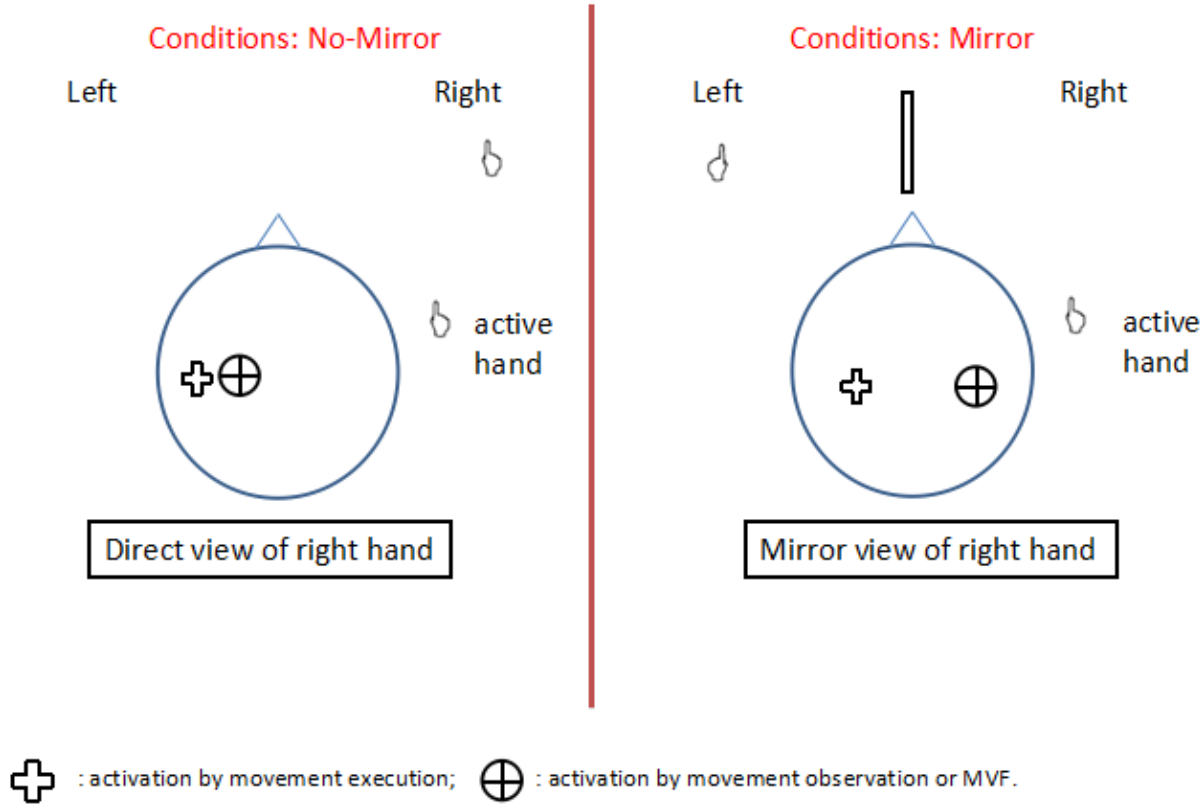

Figure 1.7 Schematic diagram of mirror visual feedback (MVF) effect. Mirror condition is on the right side. The no-mirror condition is on the left side.

Most studies which investigated the MVF effects only focused on the free movements, such as Praamstra et al (2011) did extension-flexion right or left index finger movements [36]. However, a recent study showed that goal-oriented actions would increase the cortical activation [37]. Thus, the second hypothesis is that the presence of a movement goal will amplify the effect of MVF on cortical activations.

In these two hypotheses, two factors were manipulated to form four conditions (M^+G^-; M^-G^-; M^+G^+; M^-G^+). Beta band ERD on motor cortex will be used to investigate

MVF (or mirror) effect because it is related to the movement execution. Moreover, alpha band ERD on parietal cortex will be used to explore goal effect since it is associated with goal information processing. In addition, the prefrontal cortex is selected to work as control site to prove that the MVF (mirror) and goal effects didn't come from data analysis mistakes or environmental factor.

CHAPTER 2

MATERIALS AND METHODS

In Chapter 2, experiment design, procedure and analysis methods are in detail.

2.1 Participants

Sixteen healthy adults volunteered to participate in this study. After confirming the presence of the kinematics, EMG signal and EEG signals in our testing environment, all (16 men, mean age = 22 ± 3 years) of them were chosen to participate the following test conditions. All subjects are right-handed and had normal or correct-to-normal vision. After receiving the experiments description, all subjects provided their informed consent. The subjects' information is shown in the Table 2.1.

Table 2.1 Subject Information (V = No-mirror; M = Mirror; F = No-goal; G = Goal)

16 Subjects:	First day	Second day
ML	VF & MF	VG & MG
DST	VF & MF	VG & MG
MZ	VG & MG	VF & MF
MAT	VG & MG	VF & MF
OO	MF & VF	MG & VG
AE	VF & VG	MF & MG
BEX	VF & VG	MF & MG
BJ	MF & MG	VF & VG
CM	MF & MG	VF & VG
HT	VF & VG	MF & MG
JG	VF & VG	MF & MG
KK	MF & MG	VF & VG
MB	VF & VG	MF & MG
MC	VF & VG	MF & MG
SR	MF & MG	VF & VG
YG	VF & VG	MF & MG

2.2 Experiment Design

2.2.1 Virtual Reality System

A personal computer-based virtual reality system was developed for our experiments. The virtual reality (VR) system consists of a host personal computer (PC), a slim 27-in. liquid crystal display (LCD) monitor with a revolution of 1920×1080 pixels, and CyberGlove® (Immersion Co., San Jose, CA) which worked as a hand input device. In addition, the virtual environment was developed using commercial software Virtool®. The system was shown in Figure 2.1. Subjects wearing CyberGlove® on the right hand in all conditions sat behind the screen and placed both hands on an arm rest under the screen. When subjects moved their fingers, the sensors in CyberGlove® can detect and record the continuous finger movement signals and then these signals would be sent to the personal computer. The software Virtool® in the host PC was used to process the acquired movement signals and continuously send them to the monitor. In summary, the CyberGlove® which is in conjunction with the software Virtool® and the LCD monitor constitute the VR system for our experiments. Moreover, this VR system can make the right index finger movements in accordance with the left (mirror) or right (no-mirror) index finger movements on the monitor without any delay. Before the experiment, each subject was asked to test whether the virtual hand can follow his/her real hand movements, and no delay problem was reported by subjects. Furthermore, the Virtool® software provides the ability to set movement goals (20, 40 and 60 degrees) and show movement cue (move, return and rest cue) to instruct subjects. The move cue was set as a trigger in EEG data capture system which used to extract epochs.

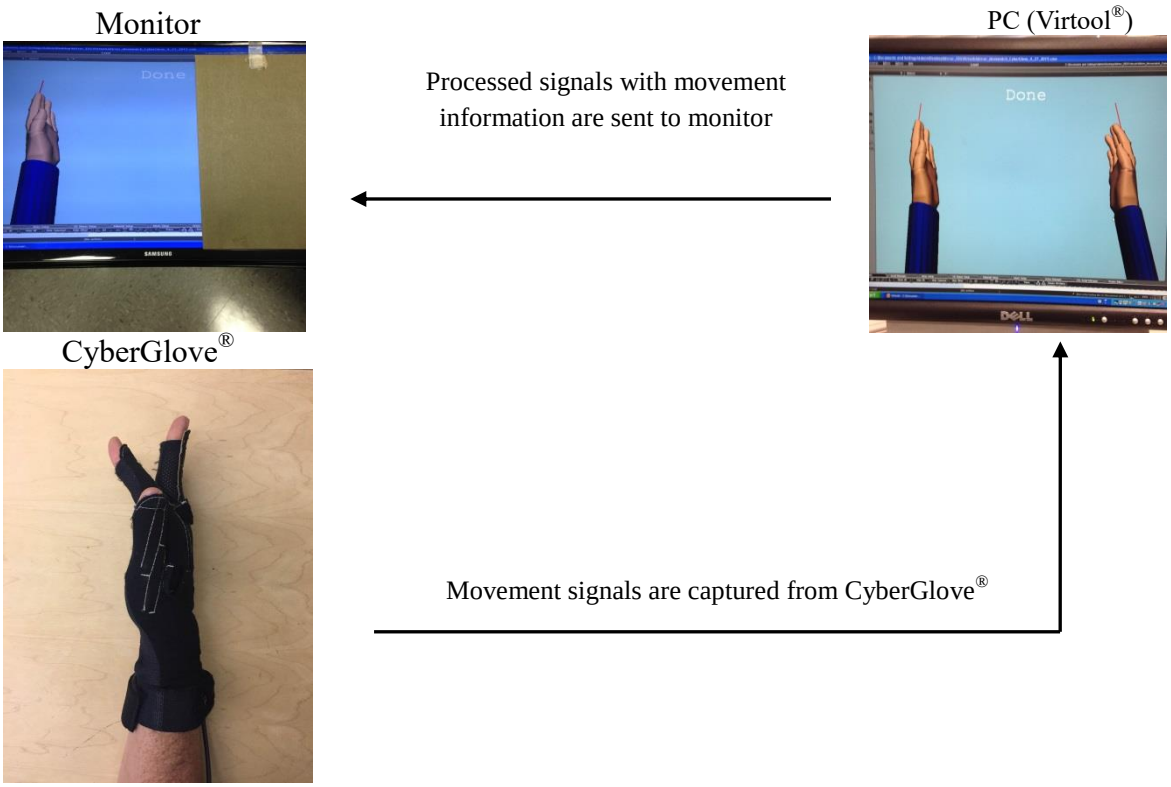

Figure 2.1 Diagram of Virtual Reality system. The Virtool® software in host PC captures signals from the CyberGlove® of the active hand. The Virtool® software then sends the processed signals with movement information (goals and cues) to monitor.

2.2.2 Test Conditions

Two factors (mirror and goal) formed four test conditions (M^+G^-; M^-G^-; M^+G^+; and M^-G^+

Figure 2.2):

1. No-goal movement with mirror visual feedback (M^+G^-), in which the subjects were asked to freely move their right index fingers after seeing the 'move' cue and received the visual feedback from the side opposite(on left) to the moving hand;

2. Goal-directed movement with mirror visual feedback (M^+G^+), in which the subjects were asked to flex their right index fingers to meet one of three goals (20, 40 and 60 degrees) after seeing the 'move' cue, and received the visual feedback from the side opposite(on left) to the moving hand;

3. No-goal movement without mirror visual feedback (M^-G^-), which the subjects were asked to freely move their right index fingers after seeing the 'move' cue while receiving the visual feedback from the same side as the moving hand;

4. Goal-directed movement without mirror visual feedback (M^-G^+), in which the subjects were asked to flex their right index finger to meet one of three goals (20, 40 and 60 degrees) after seeing the 'move' while receiving the visual feedback from the same side as the moving hand;.

All the subjects were instructed to move as quickly as possible for all four conditions and as accurately as possible for two goal-direct movements, after seeing the 'move' cue. And during the movements, subjects' left hands were keeping relaxed on the arm rest. For the goal conditions, one of three goals (20, 40 and 60 degrees) was automatically and randomly selected to show on the monitor.

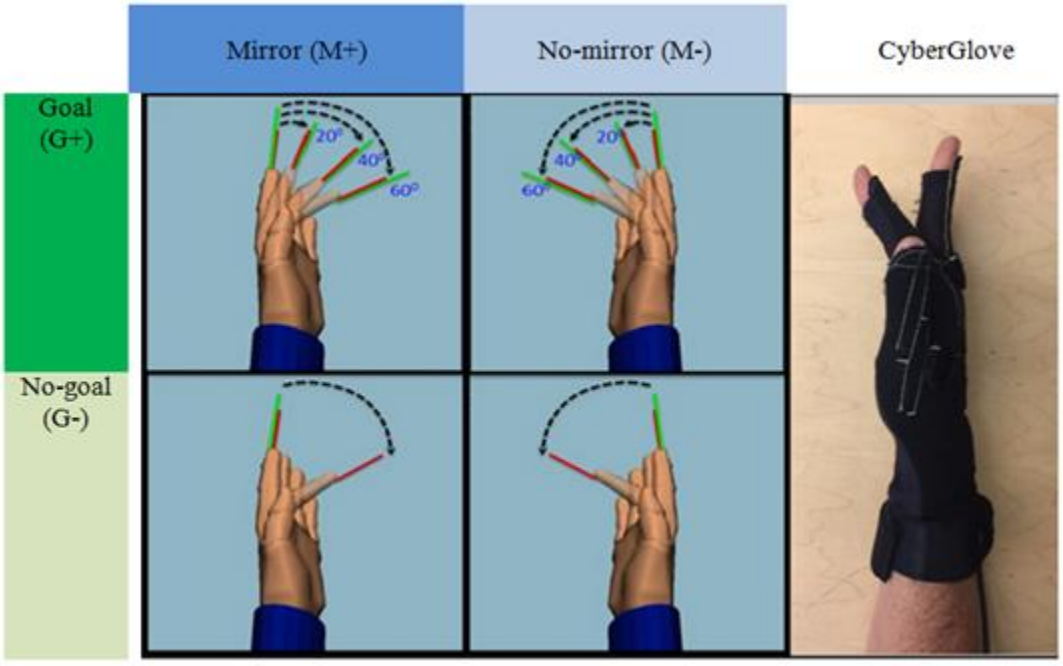

Figure 2.2 Testing conditions. All subjects were instructed to move their right index fingers after seeing 'move' cue. In the no-mirror without goal condition (M^-G^-), subjects can freely move their right index fingers, while in the no-mirror with goal condition (M^-G^+), one of three goals (20, 40 and 60 degree, green lines in M^+G^+ and M^-G^+ conditions) would be randomly shown on the screen, subjects were asked to move as quickly and as accurate as possible to get goal shown on the screen. In these two conditions, subjects will get visual feedback from the same side as moving hand. In the mirror without goal (M^+G^-) and mirror with goal (M^+G^+) conditions, subjects were asked to repeat the movements as they did in the no-mirror conditions; the only difference is that subjects will receive visual feedback from mirror side.

2.3 Experimental Paradigm

All of the experiments were conducted in the same dark room with air conditions to keep the temperatures as stable as possible. The subjects were seated in a stable chair with their forearms resting on an arm rest. And they were instructed to position their active hand similar to the virtual hand at rest. During the experiment, subjects were instructed to relax and minimized body movements in order to ensure that the EEG signals would not be contaminated by noise and artifacts. And all subjects were trained for several trials before the experimental session, which can make them to be familiar with the VR system. Each subject (right-handed) completed all four sessions on two separate days. Each experimental session was divided into 6 blocks. Except for the first and the last block, each of the resting blocks contains 30 trials. The first block (three trials) was used to make the subjects to be familiar with degrees' positions and the last block (three trials) was used to test the calibration results. The Virtool® sent different cues (move, return and rest) to the monitor which can instruct the subjects to perform specific movement. Each trial starts with presentation of a 'rest' cue. When subjects saw this cue, they will relax their body and hands. Then after 1s, the 'move' cue will be showed in the screen. Finally, the 'return' cue was used to inform subjects to move their index fingers back to the initial positions. One generic schema of the experiment session was shown in Figure 2.3. 0s was defined as move cue, 2s prior to the move cue is defined as trial start, and 2s after the move cue is defined as trial end. The whole experiment can be divided into four phases: Pre movement phase (-2s to 'move' cue); movement preparation phase ('move' cue to move onset); movement execution phase (move onset to move offset) and Post movement phase (1.5s to 2s). The four conditions are randomly selected to test subjects on the two

separate days. Between two testing conditions, subjects can take 30 min break. And between each block, subjects can take 5 min break.

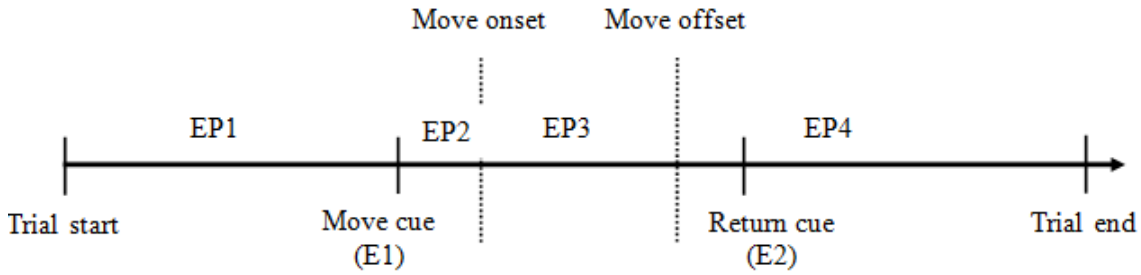

Figure 2.3 Schema of a generic VR-induced hand movements. The experiment design introduced specific task epochs: EP1 (Pre-move phase), in which subjects kept relaxing; EP2 (movement preparation phase), in which the subjects can get movement information and then prepare the movement; EP3 (movement execution phase), in which subjects flexed their index finger as quick and as accurately as possible. EP4 (Post-move phase), which is a relaxing epoch after movement completion. 0s is defined as move onset.

2.4 Data Capture

2.4.1 Kinematics

The software Virtool® supports the use of CyberGlove® (Figure 2.4) which can instrument gloves for hand tracking. The CyberGlove is a stretchable data glove with 18 embedded bend sensors that can measure the metacarpo–phalangeal and proximal interphalangeal joint angles of the thumb and fingers as well as finger abduction and wrist flexion. Hand position and orientation as well as finger flexion and abduction were recorded in real time and translated into three dimensional movements of the virtual hands shown on the screen in a first-person perspective. And all the kinematics will be analyzed using MATLAB (Mathworks Inc., Natick, MA) code.

Figure 2.4 CyberGlove. Instrumented gloves (Immersion Co., San Jose, CA) were used to track finger movements.

2.4.2 Surface EMG Data

When subjects flex their index fingers, the first dorsal interosseous (FDI) muscle will be active. To provide a reference point for the start of the movement, a pair of surface electrode (Delsys Inc., Natick, MA) was placed on the first dorsal interosseous (FDI) muscle of the active hand (Figure 2.5). The attachment location was decided by palpation of the active muscle area when the subjects were asked to flex their index fingers. And the reference point is the right elbow. The EMG signals were amplified (gain × 100) with an amplifier (Delsys Inc., Natick, MA), and were collected via a data acquisition device (PCI-6259; National Instruments Inc.) with sampling rate of 2048Hz. All EMG data were later analyzed using MATLAB (Mathworks Inc., Natick, MA) code. Before the experiment start, the EMG activity will be tested in order to make sure that the EMG signals were not contaminated by 60Hz noise.

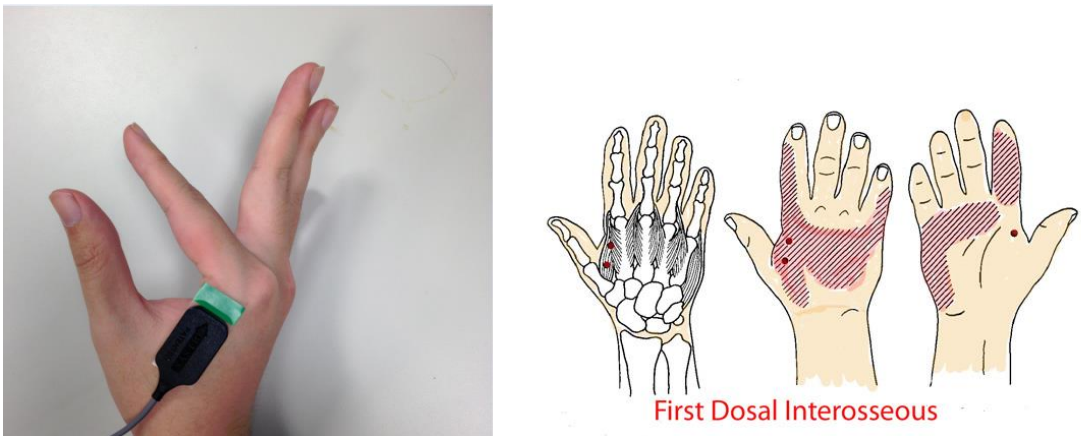

A B

Figure 2.5 EMG electrode placement. (A) Surface electromyography electrode (Delsys Inc., Natick, MA) was used to record First Dorsal Interosseous (FDI) muscle activity at 2000Hz. (B) First Dorsal Interosseous (FDI) muscle anatomy. The red dots represent the FDI muscle position.

Source: http://professionalmassagetherapist.org/trpt/trpt_Results.php

2.4.3 EEG Recording

The Non-invasive 64-channel WaveGuard™ EEG cap was used to monitor and record subjects' brain activity (Waveguard™ Active Shield, ANT Figure 2.6) with sampling rate 2048Hz. Sintered Ag/AgCl provide the best EEG signal quality of all electrode materials, and are maintenance-free. The position of Cz electrode was used as an index to ensure all electrodes' positions are correct. The impedances of all electrodes were checked using ASALAB 4.7.3 (ANT™ Software; https://www.ant-neuro.com/products/asa) and maintained below 10 kΩ. The recorded EEG signals were sent to a full-band EEG DC amplifier (Advanced Neuro technology, ANT™) with max 10,000Hz sampling rate. No online filter was used during the recording. The experimenter can monitor the EEG data on–line using ASA-lab to confirm the quality of activity, during the experiments. In

addition, because 64-channel WaveGuard™ EEG cap is 10-20 system, C3 and C4 electrodes cover the motor cortex, P3 and P4 electrodes cover the parietal cortex and Fp1 and Fp2 electrodes are selected as control sites.

A

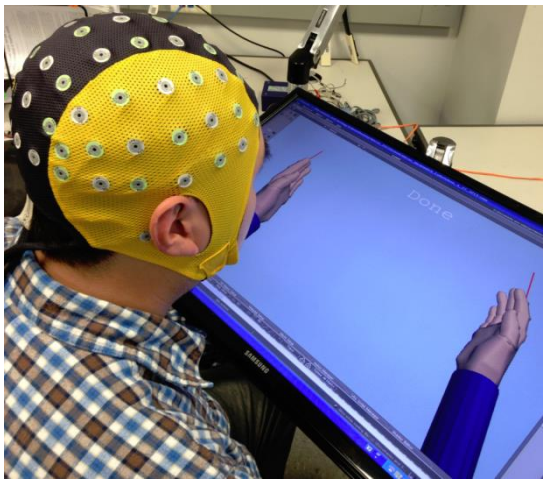

B

C

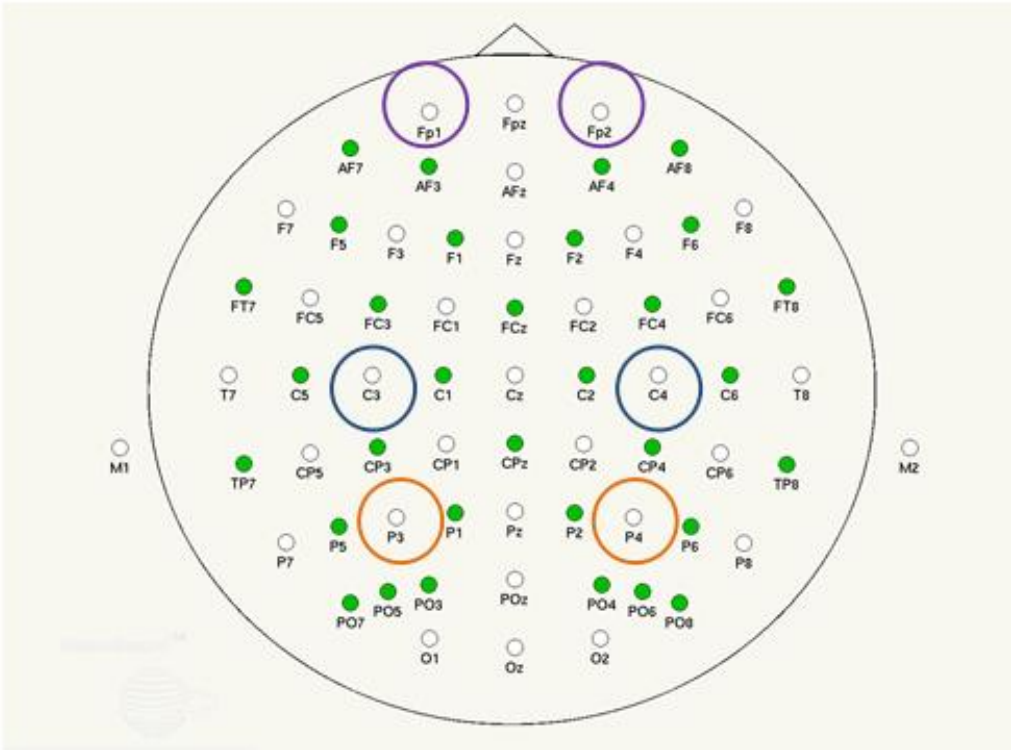

Figure 2.6 EEG setups. (A) The Non-invasive 64-channel WaveGuard™ EEG headset was used to monitor subjects' brain activity. (B) A full-band EEG DC amplifier for 64 channels EEG system. (C) EEG electrode placement.

2.5 Data Analysis

2.5.1 Kinematics Analysis

Raw data was filtered by a Gaussian low-pass filter ($\delta = 6$) and then increasing the original sampling rate to 1000Hz. The movement offset of each trial was defined by the five percent of the peak velocity (Figure 2.7) [18]. Bad movement trials were determined by visually checking trajectory trial by trial. Then these bad trials were rejected.

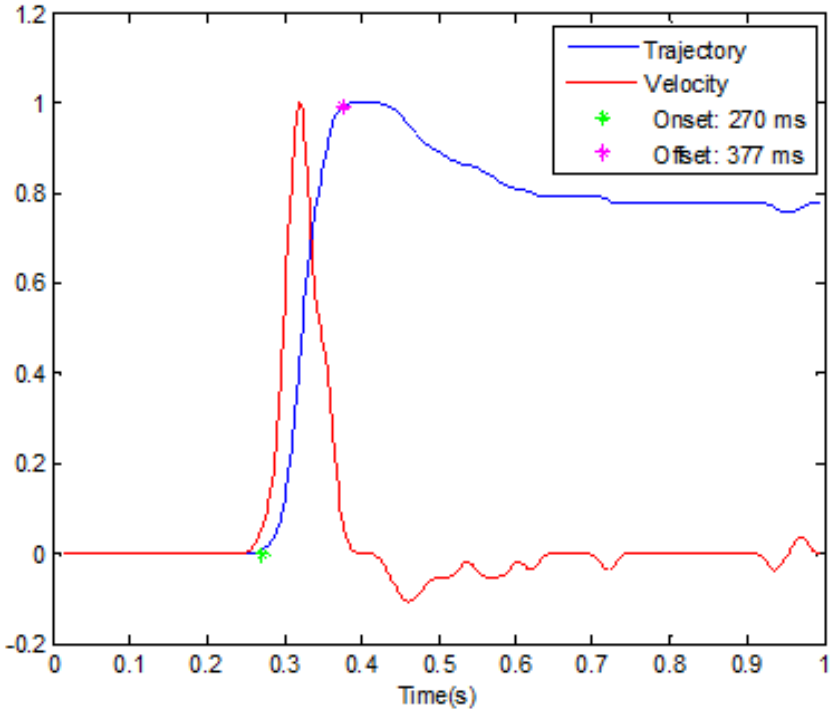

Figure 2.7 Kinematics graph. The graph showed the normalized trajectory of index finger movement (blue) and normalized velocity (red) corresponding to this movement. The purple dot represents the move offset which is defined by the five percent of the peak velocity.

2.5.2 EMG Data Analysis

The original EMG signals were preprocessed by a band-pass filter (2^{nd} order, 10 – 300Hz) and a band-stop filter (2^{nd} order, 55 – 65Hz). Then, the processed EMG signals were removed mean value and rectified. The application of the root mean square (RMS) filter (T_m=30ms) to the processed EMG signals produced the EMG envelope (figure 2.8). The EMG signal can be used to determine the time of muscle activation. A standard approach for muscular activity starting time estimation is based on the times at which the envelope of the signal exceeds a threshold. The threshold is given by

$$Threshold = \mu + J\sigma \tag{2.1}$$

where μ and σ are the mean and standard deviation of the envelope during a phase of inactivity, and J is a constant [19]. Here, J=3. And the inactivity phase in this experiment is from 3s to 3.5s after 'move' cue. If the onset is incorrect, it will be manually changed by corresponding kinematics onset. And all bad trials of EMG signals were rejected. Also, movements that start very early in the trail were also rejected as well because these move onsets came from prediction of the movement instead of the cue instructed movement.

A

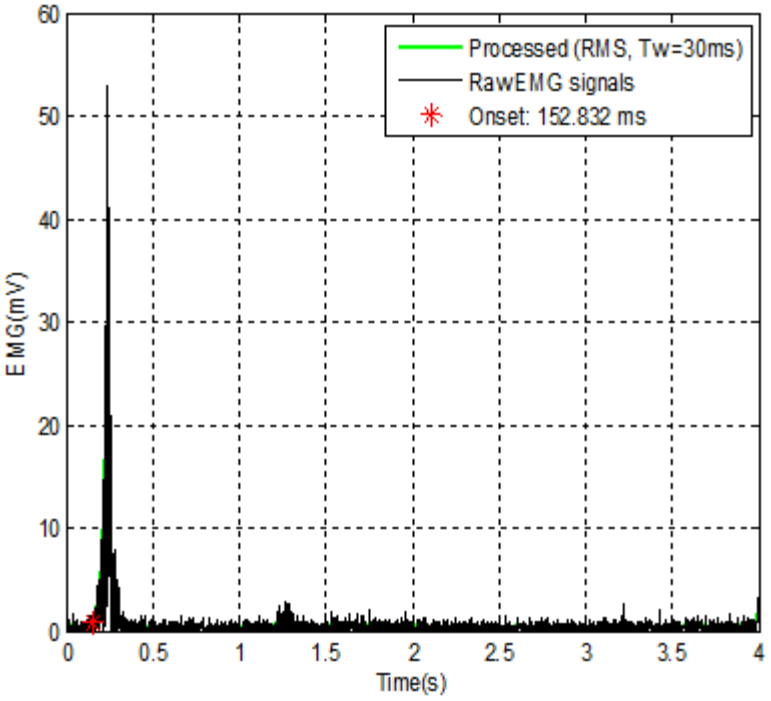

B

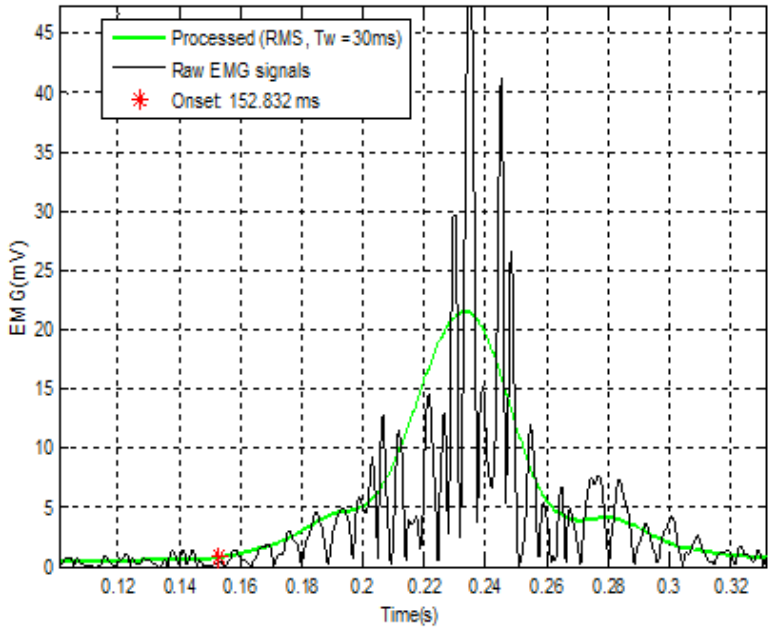

Figure 2.8 Processing of EMG signals. (A) The application of the root mean square (RMS) filter on the EMG signal is shown above. (B) A zoomed in graph of first dorsal interosseous (FDI) muscle activity. The red star represents the move onset.

2.5.3 EEG Data Analysis

One available EEGLAB (Figure 2.9) toolbox (http://www.sccn.ucsd.edu/eeglab/), running under the platform MATLAB environment (Mathworks, Inc., Natick, MA), was used to preprocess the raw EEG signals. All the preprocessing methods can be finished in EEGLAB toolbox and some homemade MATLAB (Mathworks, Inc., Natick, MA) scripts.

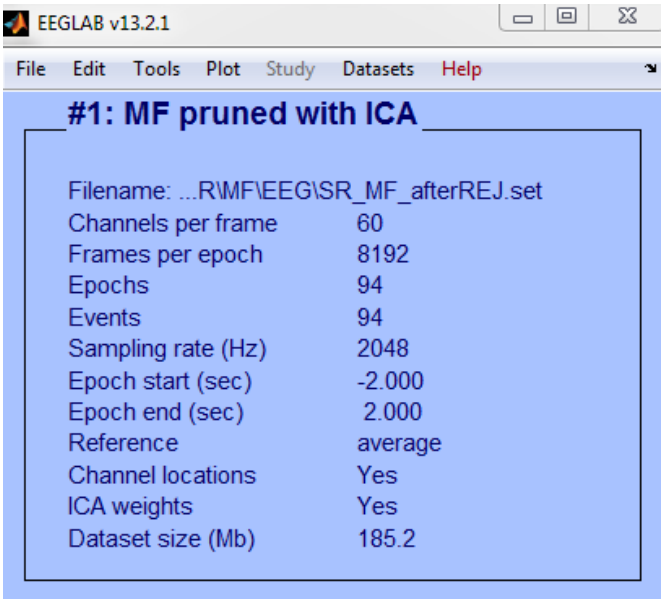

Figure 2.9 Sample EEGLAB environment. The basic information can be learned from the panel, such as sampling rate, etc.

2.5.3.1 Preprocessing. EEG data were analyzed offline using EEGLAB (http://www.sccn.ucsd.edu/eeglab/). Firstly raw EEG data, event information, and channel location files were imported in the EEGLAB tool. Then EEG signals in all channels were re-referenced using average reference. After that, EEG signals were filtered by a band-pass filter (2^{nd} order, 1– 70Hz) and a band-stop filter (4^{th} order, 55 – 65Hz), which would remove 60Hz line noise. To study the event–related EEG dynamics from continuously recorded data, epochs were extracted based on the move cue. Next, a

mean baseline value from each trial was removed because of the inter-trials baseline differences. Channel M1 and M2 were rejected due to these two electrodes recorded much auditory noises during experiments. Figure 2.10 display the pre-processing steps. Finally, EEG activations were manually checking one trial at a time. If one trial's amplitude exceeded ±100μV, this trial will be excluded. Figure 2.11 showed two trials of the EEG activities after processing. However, after preprocessing, there also exist some artifacts which have similar frequency which cannot be filtered by Butterworth filter. To solve this problem, independent component analysis is a powerful tool.

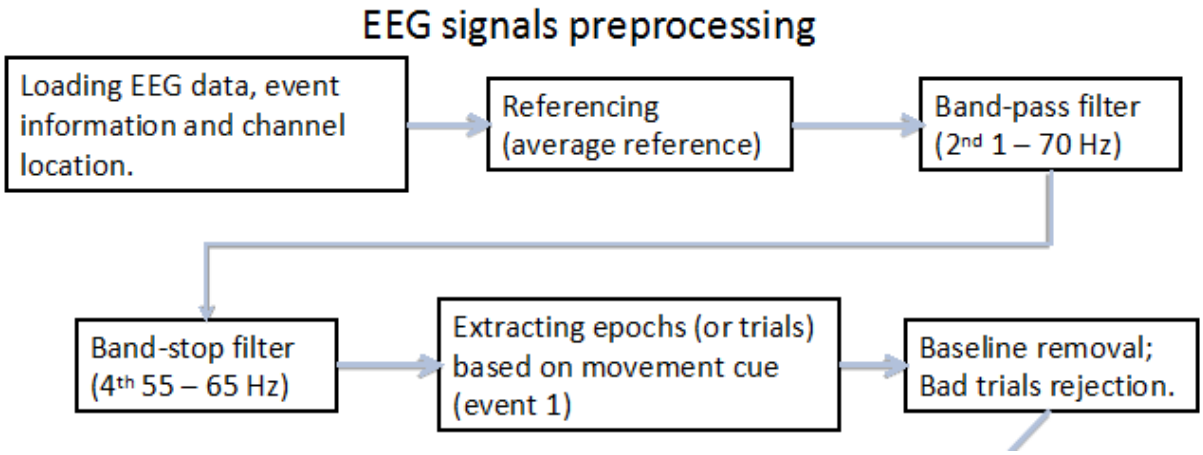

Figure 2.10 EEG signals preprocessing (six steps). All the steps can be automatically finished based on homemade MATLAB code and EEGLAB.

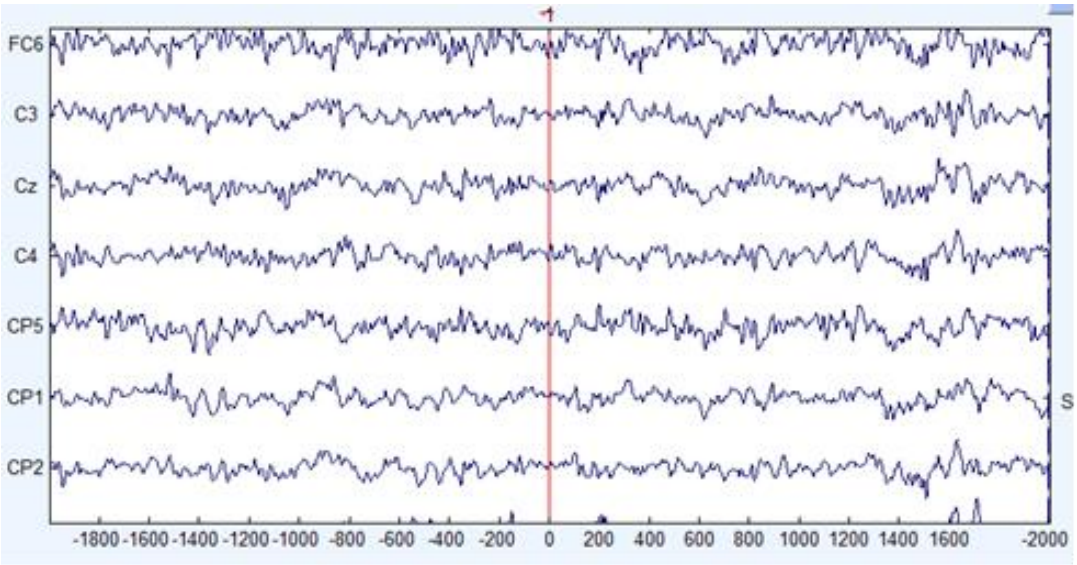

Figure 2.11 EEG activities after preprocessing. The screen shot showed one trial EEG signals on several channels (y axis) over time from -2s to 2s (x axis). Inside, the red vertical line is event 1 ('move' cue).

2.5.3.2 Independent Component Analysis (ICA). If there is an array of microphones records mixtures of the voices of several people talking at once at a cocktail party, how would you separate the real voice from indecipherable 'cocktail party noise'? This is the famous 'cocktail party problem' (Figure 2.12).

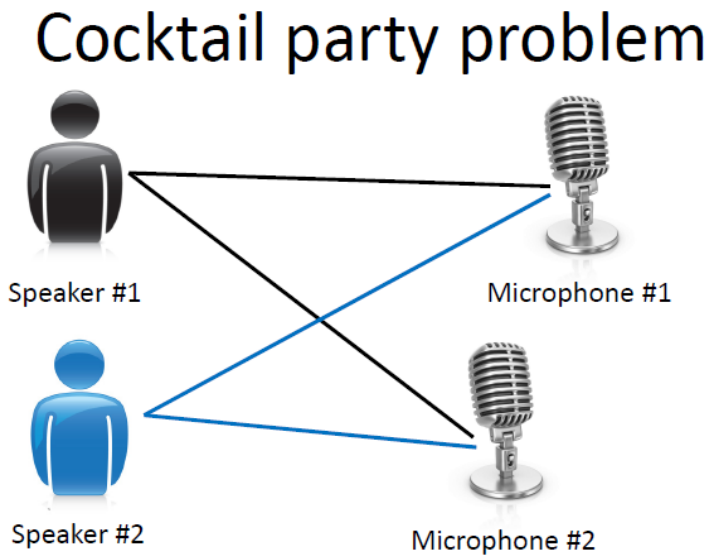

Figure 2.12 Cocktail party problem. Microphone 1 and microphone 2 recorded mixture signals came from speaker 1 and speaker 2.

The key point in this problem is that no prior information about the source signals or the mixing process is available. Thus, the solution to this blind source separation (BSS) problem is finding out a matrix *w* to maximally reverse the mixing effect [20]. As to matrix *w* calculation, independent Component Analysis (ICA) is one of the most popular method recently. By applying randomly weight matrix (*w*) on the recorded signals to make the mixed signals more and more temporally independent of each other, this unmixing process must finally get the individual voice signals. And this procedure called independent component analysis (ICA). In other words, the mixing microphone data can be finally separated into its maximally independent signal components. More technically, independent time series have no mutual information, meaning that knowing the value of one component at a given time gives no information at all about the concurrent value of the other process. Figure 3.13 schematically visualizes a simple matrix algebraic formulation of the linear signal decomposition used in ICA. ICA applied to a matrix of EEG channel data (upper middle) finds an 'unmixing' matrix of weights (*w*, upper left) that, when multiplied by the channel data matrix (*X,* upper middle), gives a matrix of independent components activation (*a*, lower right). This is the process of ICA decomposition (downward arrow) of the data into maximally and temporally independent signals, each with its distinct time series and scalp map. The process of back – projection (upward arrow) reforms the original channel data by multiplying the IC activation matrix (*a*, lower right) by the matrix of independent component (IC) topographies (w^{-1}, lower center) whose columns give the relative projection weights from each component to each scalp channel. The IC topographies or 'mixing' matrix (w^{-1}, lower center) is the inverse of the 'unmixing' matrix (*w*, upper left).

In this simple ICA algorithm form, if the channel data matrix is X and the independent component activation matrix is a then the observed signals can be written as,

$$wX = a \tag{2.2}$$

X represents a mixing matrix with the size of $n \times n$, and a is the matrix of independent components. The aim of ICA is to find a matrix w to separate the mixed signals. Then, after computing the matrix w, we can obtain the independent components by

$$X = w^{-1}a \tag{2.3}$$

Technically, the ICA could be regard as a spatial filter [21].

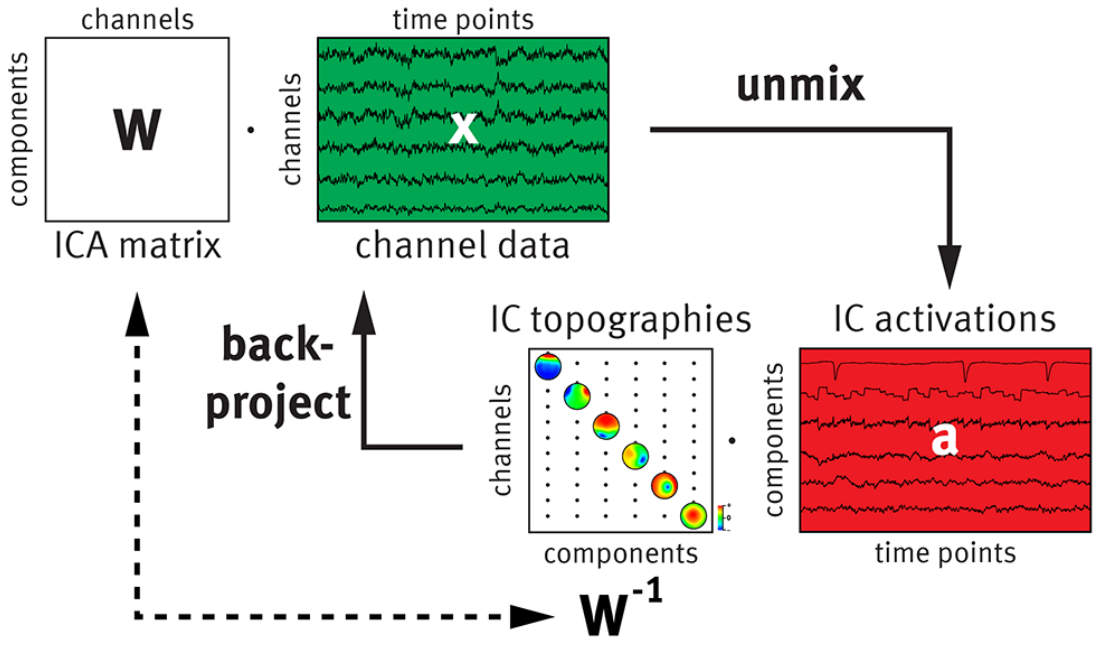

Figure 2.13 Schematic flowcharts of independent components analysis data unmixing and back-projection. ICA unmixing and back-projecting using six EEG channels resulted in six independent components, each with a specific IC activation and topography. This general schematic holds for all linear decomposition methods returning as many components as there are data channels.

Source: Plank, Markus. "Independent Component Analysis–demystified!."

Based on the features of ICA, Makeig et al. (1996) firstly applied ICA on the EEG signals, which performed the first decomposition of EEG signals into its maximally independent components [22]. Here, *w* is a matrix of spatial filters learned by ICA from the EEG channel data. Then it was applied to the data to find the activity projections of the underlying EEG source processes and the IC activation. Currently, ICA was widely used in the EEG research, most often to detect and remove eye blink, muscle, and line noise artifacts. Many ICA algorithms are developed and used in decades such as Infomax, JADE, FASTICA, etc. [21]. Infomax algorithm is based on the general optimization principle for neural networks and other processing systems described by Linsker in 1987 [23]. The Infomax algorithm for calculating independent components is based on the maximization of the output entropy of a neural network with non-linear outputs. The weights of this neural network are updated according to the following formula:

$$w_{k+1} = w_k + \mu_k[I - 2g(y_k)y_k^T]w_k \tag{2.4}$$

y is matrix of source estimation; *k* is number of iteration; *I* is the identity matrix; μ_k is the learning rate which may depend on *k*; *g* (.) is a nonlinear function. Mostly, the nonlinear function is always calculated by,

$$g(y) = \frac{1}{1+e^{-y}}, \tag{2.5}$$

The build–in function in EEGLAB [24], *runica (),* and its default ICA algorithm, Infomax algorithm, were used to analyze all conditions for all 15 subjects. After ICA, EEG signals will be separated into the same number independent components (ICs) as the number of channels. The Figure 2.14 and Figure 2.15 illustrated scalp maps, spectra, ERP image plots and corresponding independent activities for six typical independent artifacts,

respectively.

1) Eye blink artifact:

   This component always comes from prefrontal lobe and has kind of dramatically changes in the independent components activation plot;

2) Eye movement artifact:

   When one subject was moving his/her eyes, a horizontal dipole will be formed which is always located in the supper frontal lobe;

3) Muscle artifact:

   This component is spatially localized and show high power at high frequencies (20–50 Hz and above) as shown below (C and D) [25];

4) “Bad channel” artifact;

   This component is always localized at around one channel. And in the ERP image plots, it always contains the sudden changes;

5) “ECG” artifact:

   This component always concentrated at one channel and spikes (red dots) randomly distributed in the ERP image plots.

These six typical artifacts patterns were used to detect and determine bad independent components on all subjects and conditions.

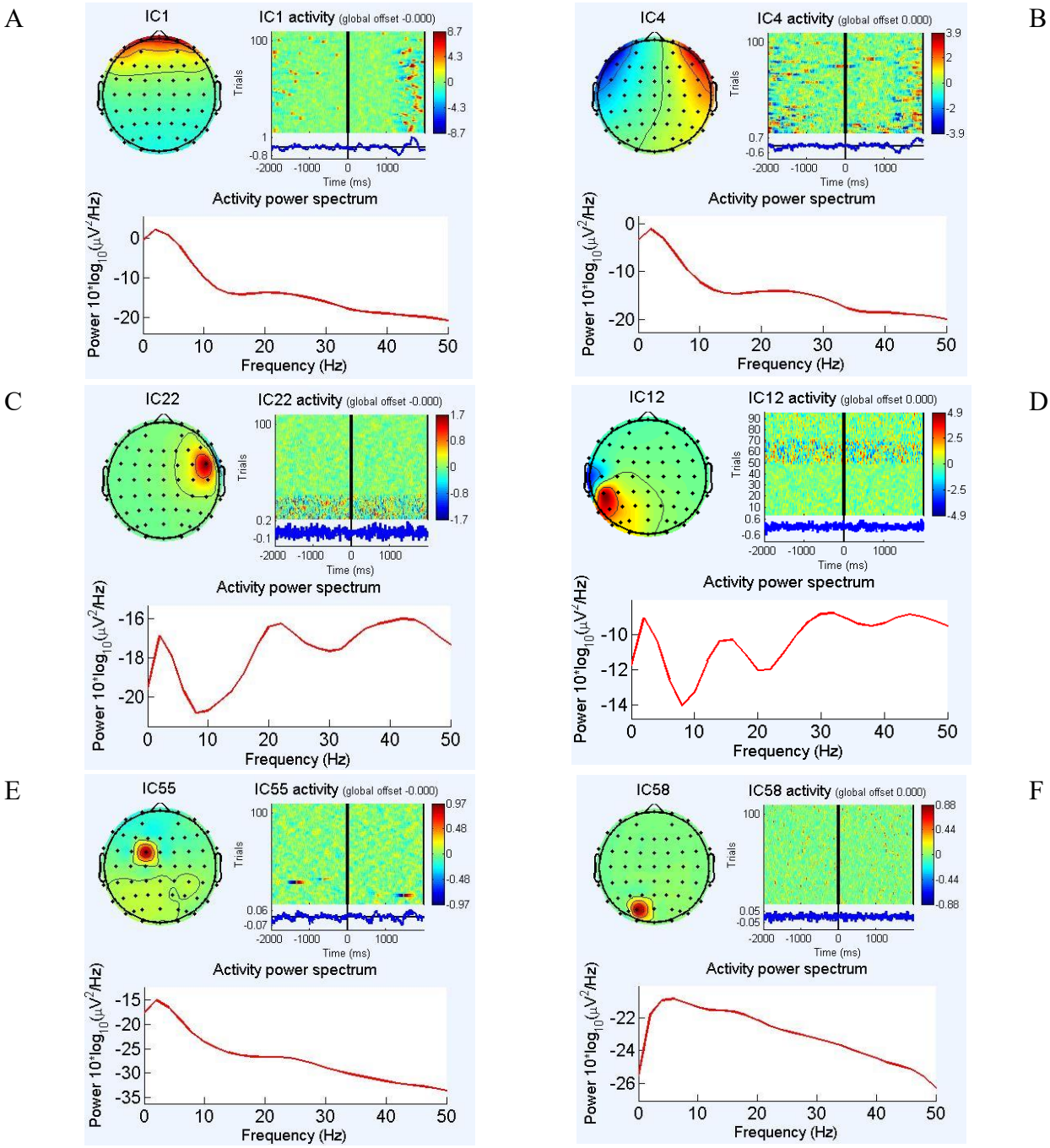

Figure 2.14 Typical component properties of six non-brain independent components. These components are shown in the order of: eye blinks (A), horizontal eye movements (B), facial muscle contraction electromyographic (EMG) activity (C and D), 'bad channel' activity (E), and electrocardiographic (ECG) activity (F), respectively.

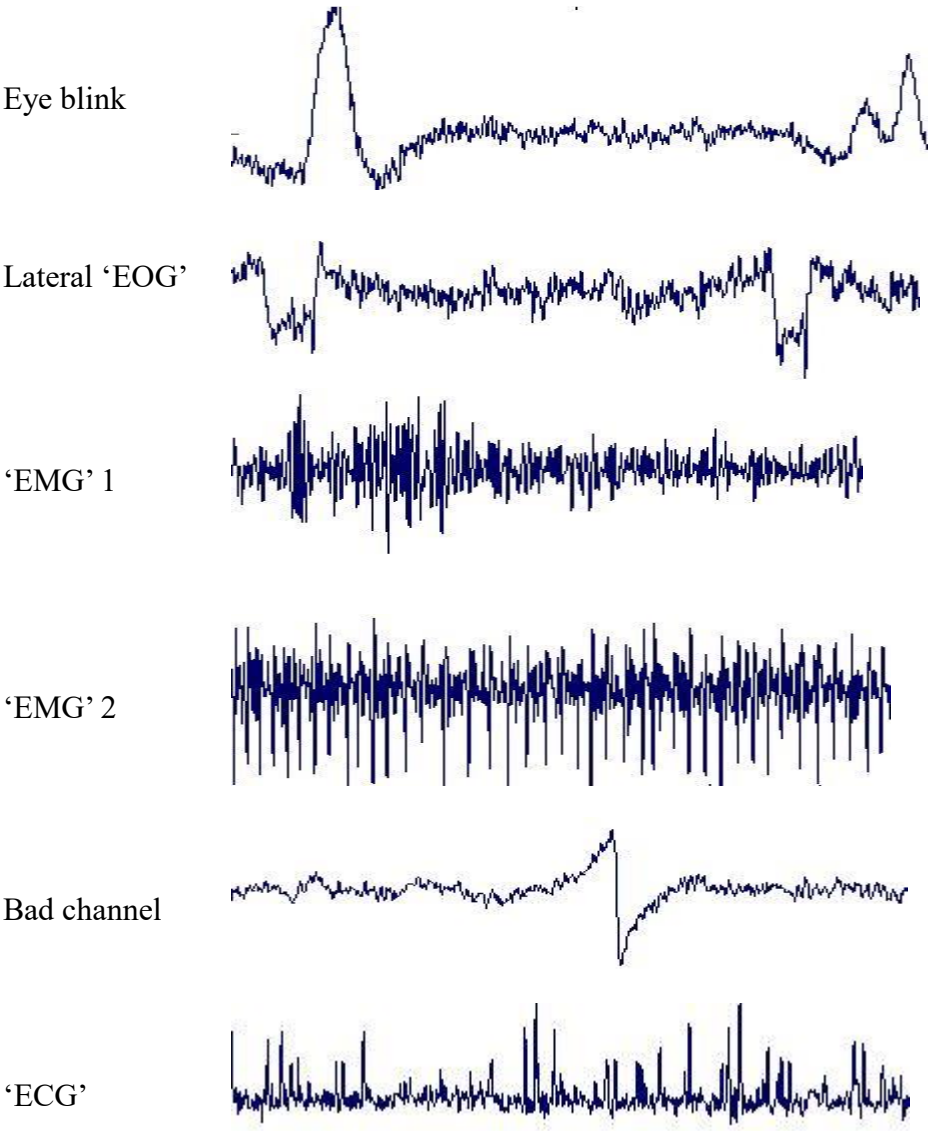

Figure 2.15 Independent activities of six bad components. From the top to the bottom, each component has a specific activity pattern, such as 'eye blink' artifact showed dramatically changes over time.

2.5.3.3 Time course of ERD/ERS. Event–related Desynchronization or Event–related Synchronization (ERD/ERS) measured the EEG power changes within identified frequency bands relative to the power of the same EEG derivations recorded during the reference phase a few seconds prior to the events occurred.

Based on the 10-20 system of EEG electrodes placing, C3 and C4 electrodes

located at around left and right motor area, respectively. Thus, the EEG signals of these two electrodes were analyzed within the beta band using 'band power' method. P3 and P4 electrodes located on top of the left and right parietal cortex. So, the EEG signals of these two electrodes were analyzed within the alpha band using 'band power' method. However, the right finger movement would not impact the two electrodes (FP1 and FP2) which are located at the prefrontal lobe were chosen as control sites. Because the reactive frequencies are specific to each subject and determination of subject–specific frequency bands is one of the most important questions for the ERS/ERD analysis. The upper and lower limits of the band-pass filter are depending on power spectrum. In Figure 2.16, significant activities of C3 and C4 electrodes ranged from 20 – 30 Hz and significant activities of P3 and P4 electrodes ranged from 9.5 – 13 Hz. Even though the reactive frequency bands are different between subjects, the reactive frequency bands for one subject in 4 conditions should be similar.

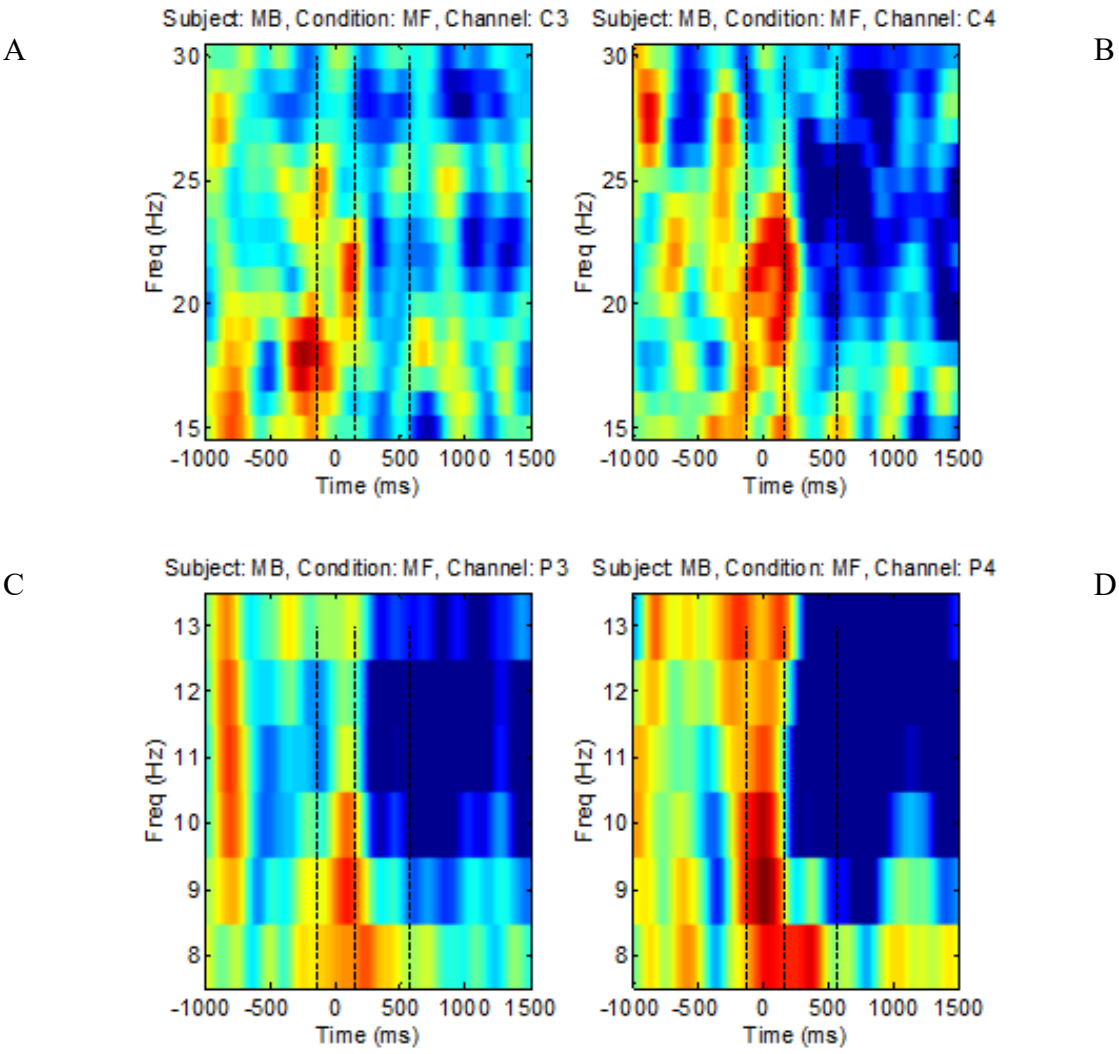

Figure 2.16 Subject-specific frequency band determination (Subject: MB; condition: $M^{+}G^{-}$). A displayed the spectrum in beta band (15–30Hz) at channel C3 and B is for channel C4. C showed the spectrum in alpha band (8–13Hz) at channels P3, D is for channel P4. Color scale ranges from 'blue' (minimum) to 'red' (maximum). Three vertical dash lines represent move cue, move onset and move offset, respectively. ($F = G^{-}$)

After the subject–specific frequency band determination, EEG signals were synchronized trial by trial using the move onset which determined from EMG signal. EEG signals were filtered within the selected band using a Butterworth band–pass filter (order = 5). Then squaring for each data point to calculate power within the specific band.

Finally averaging across trials and smoothing to obtain the clean power signals. Furthermore, the relative power of the ERS/ERD was calculated as follows:

$$\text{ERS/ERD (\%)} = \frac{(A - R)}{R} \times 100 \tag{2.4}$$

A is the power within the frequency band of interest, whereas *R* is the preceding baseline [10]. ERD is defined as power decrease and ERS as power increase. In the current study, most subjects and conditions exhibited a higher power amplitude from 1.5s to 0.5s before the index finger flexion. Thus, the average power amplitude from 1.5s to 0.5s was chosen as the reference (*R*) time window in each condition. The total procedure of relative power calculation is displayed below. Notice, because the reaction time of each trial is variable, the trials averaging will reduce the amplitude. To overcome this problem, EMG onsets were used to synchronize EEG activity (Figure 2.17 A).

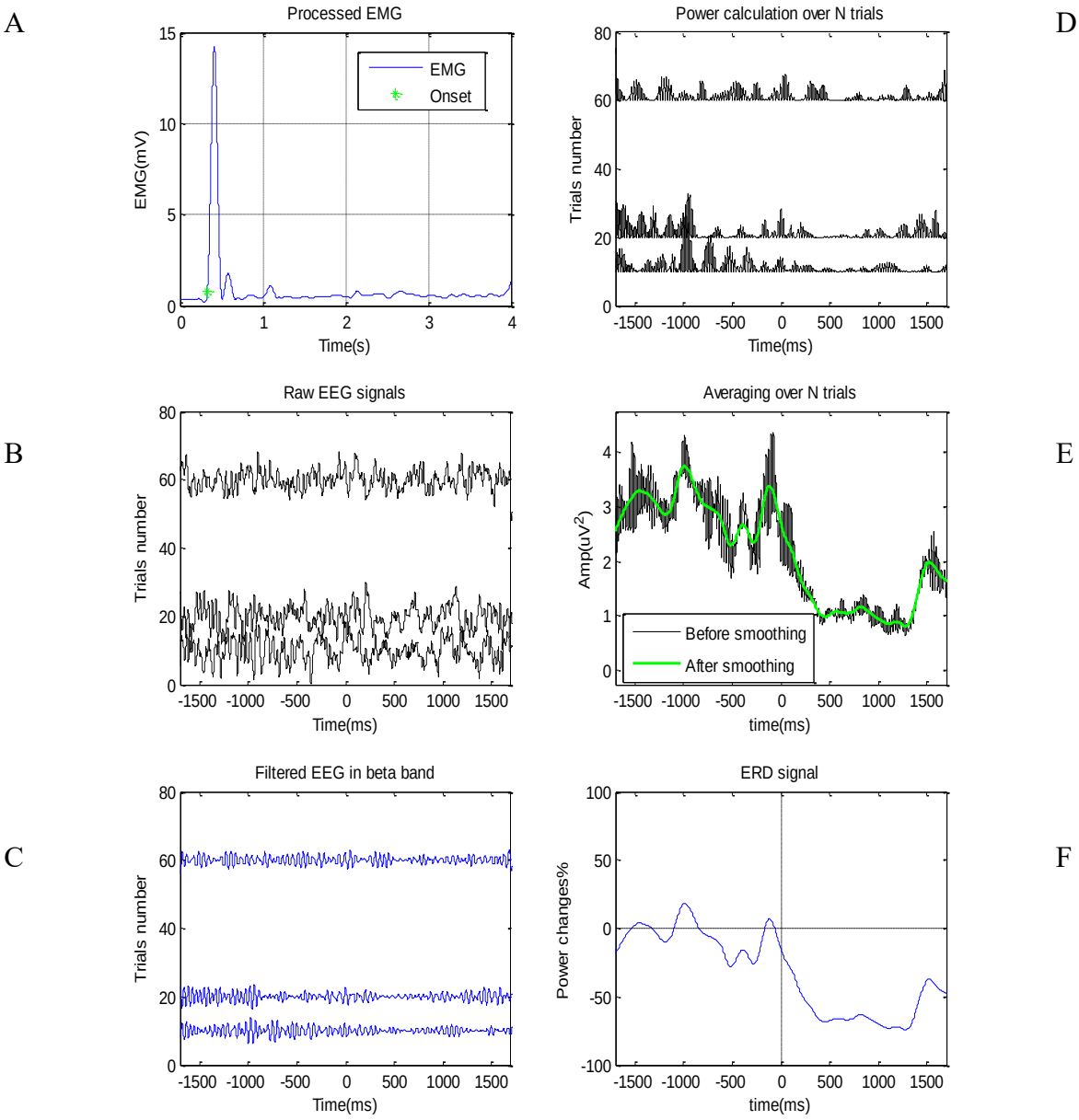

Figure 2.17 Processing of the Event-Related Desynchronization. (A) The processed EMG was used to define the move onset, the green dot is determined by the threshold of mean plus 3 times the standard deviation of the EMG signal in the time window 3s to 3.5s; (B) EEG signals in trials are synchronized by move onsets; (C) Filtering the EEG signals by trials for the beta rhythm; (D) Squaring the filtered EEG signals to obtain power signals; (E) Averaging power signals over trials and smoothing; (F) The beta-band ERD. A decrease of band power indicates the ERD. And the 0ms represents the move onset.

2.5.3.4 Sum of Squared Error (SSE). Sum of squared error (SSE) is the sum of the squared differences between each observation and its group's mean or two observations. It can be used as a measure of variation within a cluster. The formula for SSE is,

$$SSE = \sum_{k=1}^{n} (X_k - Y_k)^2 \tag{2.5}$$

X and Y represent EEG activity of two different channels, and k is the samples in the epoch [26]. From the experiment diagram, the whole time course can be divided into 4 phases: pre-move phase; movement preparation phase; movement execution phase and post-move phase. Thus, the SSE were calculated for three pairs of electrodes (C3 and C4; P3 and P4; FP1 and FP2) in different phases.

2.5.3.5 Global Topographic Measurement. Global field power (GFP) is one of the measures of global activity [27]. It is defined as,

$$GFP = \sqrt{\frac{\sum_{i=1}^{N} (u_i - \overline{u})^2}{N}} \tag{2.6}$$

Where u_i is the voltage at the electrode i, N is the average voltage of all electrodes and is the number of electrodes. GFP is the standard deviation of all electrodes at a given time. Scalp maps with steep gradients will result in high GFP, while GFP is low if scalp maps have shallow gradients (Figure 2.18). Displaying GFP over time allows to identify component latency of high SNR (signal-to-noise ratio), corresponding to moments of high global neuronal synchronization [28, 29]. However, we should note that GFP cannot be used to distinguish scalp maps between conditions. For instance, in Figure 2.18, scalp map B has a higher GFP value than A, but these two topographies are similar. And scalp

map A and C have the same GFP, however, different scalp potential distribution. In other words, without scalp maps plotting, it's meaningless to conclude any topographic difference between conditions only based on GFP value. Furthermore, after the determination of component latency, the *topoplot()* function of the EEGLAB MATLAB toolbox (Delorme and Makeig, 2004) can be used to display the topographical of EEG activity.

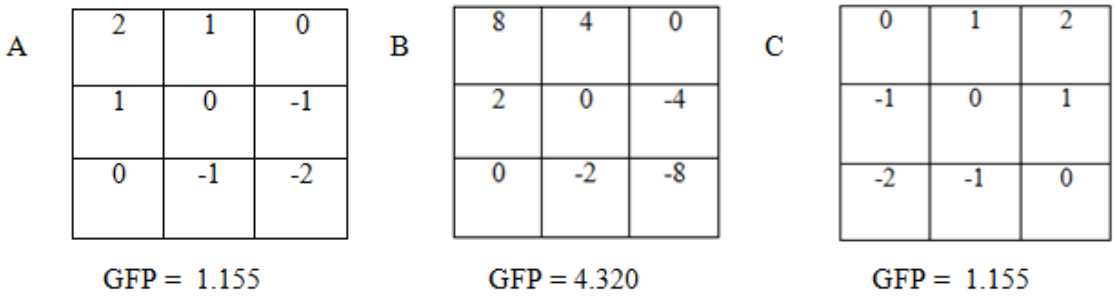

Figure 2.18 Schematic diagram of GFP interpretation. The numbers in the box of each condition (A, B and C) represent the cortical potentials at one moment of time. Condition B has a higher GFP value than A because of its higher gradients. Conditions A and B have the same GFP value but total different potential distributions.

CHAPTER 3

RESULTS

3.1 Grand Averaged ERS/ERD in Beta Band

The beta-band oscillations (ERD) at electrodes C3 and C4 were selected to analyze because they covered the left- and right- motor cortex separately. And the beta band (~15-30Hz) were used to analyzed subjects' performance underlying different testing conditions (mirror vs. no-mirror conditions) because they are prominent during movement execution.

Figure 3.1 shows the grand average time-courses beta ERD at electrodes C3 (blue curve) and C4 (red curve) for four conditions. In channel C3, a decrease in beta power (ERD) occurred at around the 'move' cue and the then the relative power activity recovered to the reference level after movement. But for channel C4, the decreases in beta power (ERD) occurred much earlier in two mirror conditions ($M^{+}G^{-}$ and $M^{+}G^{+}$) than two no-mirror conditions ($M^{-}G^{-}$ and $M^{-}G^{+}$). Furthermore, more beta-band power reductions from contralateral cortex (left hemisphere, electrodes C3) can be observed in both no-mirror conditions ($M^{-}G^{-}$ and $M^{-}G^{+}$). But for two mirror conditions ($M^{+}G^{-}$ and $M^{+}G^{+}$), the power decreases were similar at both hemispheres. At around 1.5s after the movement onset, the power amplitude recovered to the reference level (~ 0%) which might mean the cortex reached the resting state.

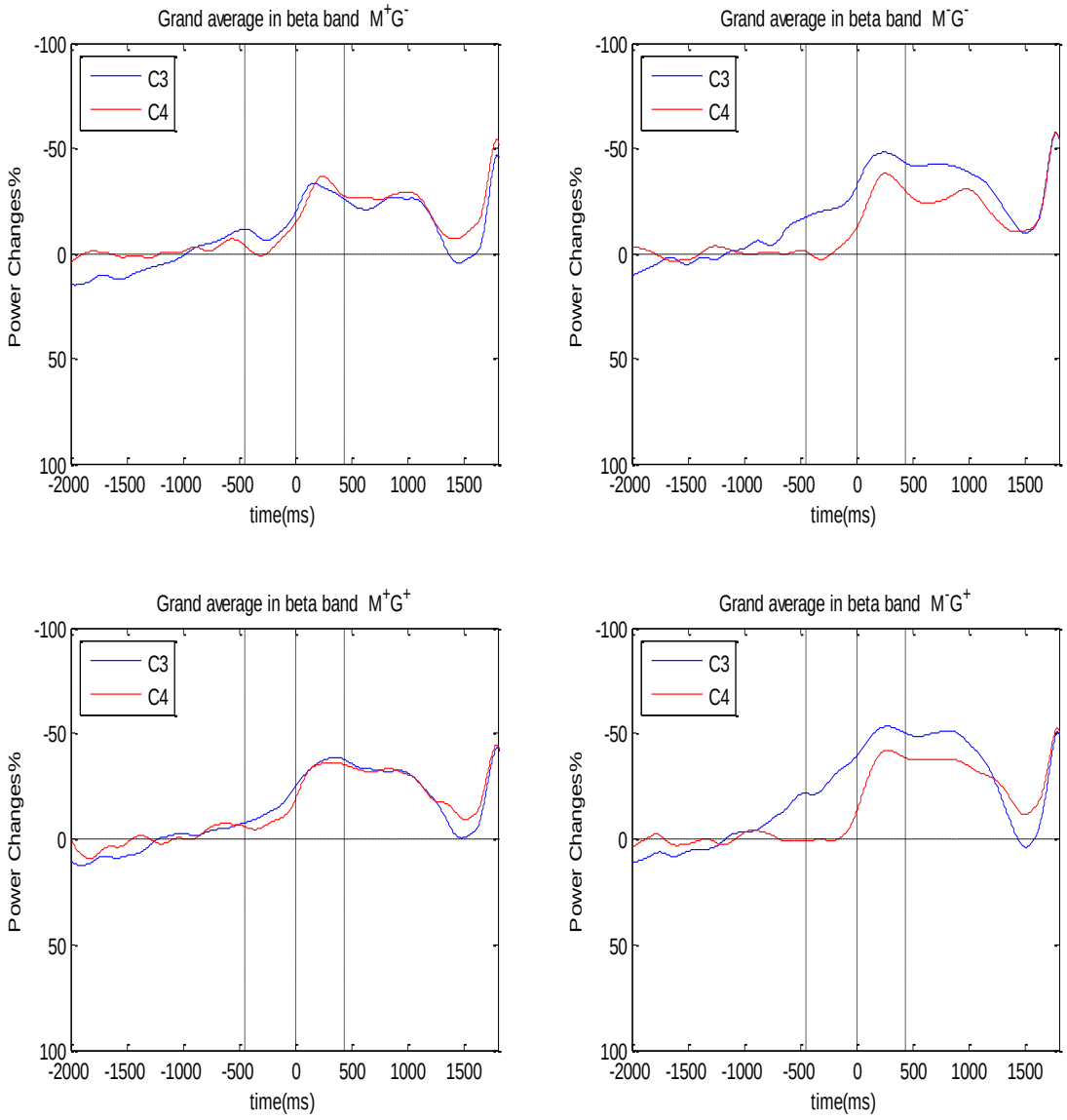

Figure 3.1 Grand average time-courses beta ERD at electrodes C3 (blue line) and C4 (red line). Four conditions (M^+G^-, M^-G^-, M^+G^+ and M^-G^+) are shown separately. Time 0 indicates movement onset and the first dash line which is before the 0ms indicated the 'move' cue and the last dash line represents the movement offset. An upward deflection indicates power decrease (ERD).

3.2 Grand Averaged ERS/ERD in Alpha Band

The alpha-band power changes (ERD) at electrodes P3 and P4 were selected to analyze because they covered the left- and right- parietal cortex separately. And the alpha band (~8-13Hz) were used to analyzed subjects' response underlying different testing conditions (goal vs. non-goal conditions) because they are prominent during the cognition process.

The grand average time-courses of the alpha-band ERD at electrodes P3 (blue curve) and P4 (red curve) for four conditions (M^+G^-, M^-G^-, M^+G^+ and M^-G^+) were presented in Figure 3.2. In channels P3 and P4, a decrease in alpha power (ERD) occurred after the 'move' cue and the power amplitude didn't recover to the reference level (~ 0%) even though the movement was completed. As to the two goal conditions (M^-G^+ and M^+G^+), the ERD occurred earlier than the two non-goal conditions (M^-G^- and M^+G^-) and all conditions' ERD waveforms are similar at both hemispheres. Interestingly, during the preparation phase, the inter-hemispheric activation (ERD) difference between electrodes P3 and P4 in M^-G^+ condition was larger than that in M^+G^+ condition. But for the execution phase, the above phenomenon disappeared.

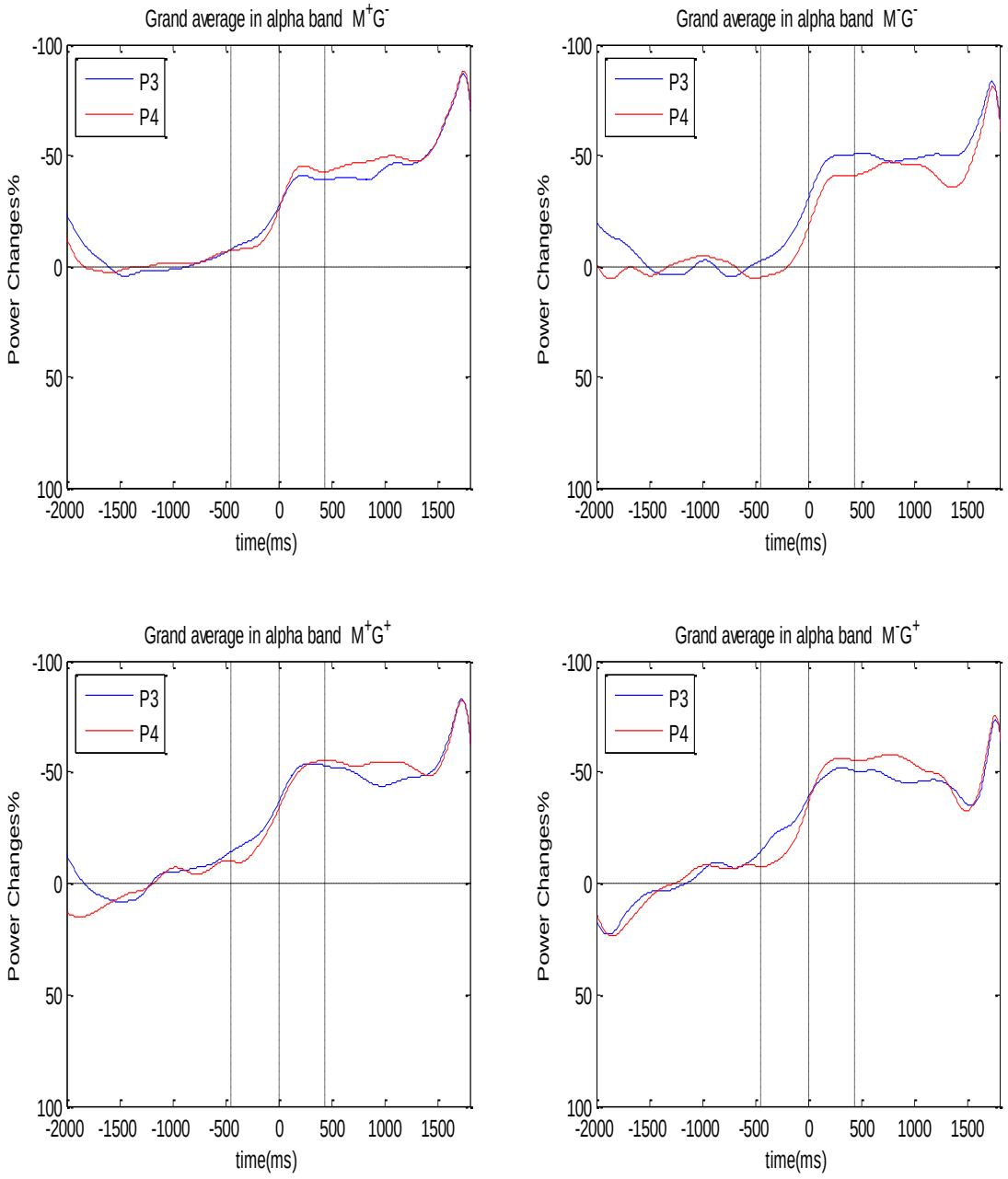

Figure 3.2 Grand average time-courses alpha ERD at electrodes P3 (blue line) and P4 (red line). Four conditions ($M^{+}G^{-}$, $M^{-}G^{-}$, $M^{+}G^{+}$ and $M^{-}G^{+}$) are shown separately. Time 0 indicates movement onset and the first dash line which is before the 0ms indicated the 'move' cue and the last dash line represents the movement offset. An upward deflection indicates power decrease (ERD).

3.3 Grand Averaged ERS/ERD on Control Sites

Figure 3.3 presented the grand average time-courses of the beta-band ERD at electrodes FP1 (blue curve) and FP2 (red curve) in four conditions (M^+G^-, M^-G^-, M^+G^+ and M^-G^+). These two electrodes are located in the pre-frontal lobe, which cannot be impacted by the right index finger movements. Thus, these two channels were selected to work as control sites. All conditions' ERD waveforms showed that after the 'move' cue, beta-band oscillations started decreasing and after 1.5 seconds, the power went back to the baseline (~ 0%). Moreover, for all conditions (M^+G^-, M^-G^-, M^+G^+ and M^-G^+) and whole phases (pre-movement phase, preparation phase, execution phase and post-movement phase), no inter-hemispheric activation (ERD) difference can be observed.

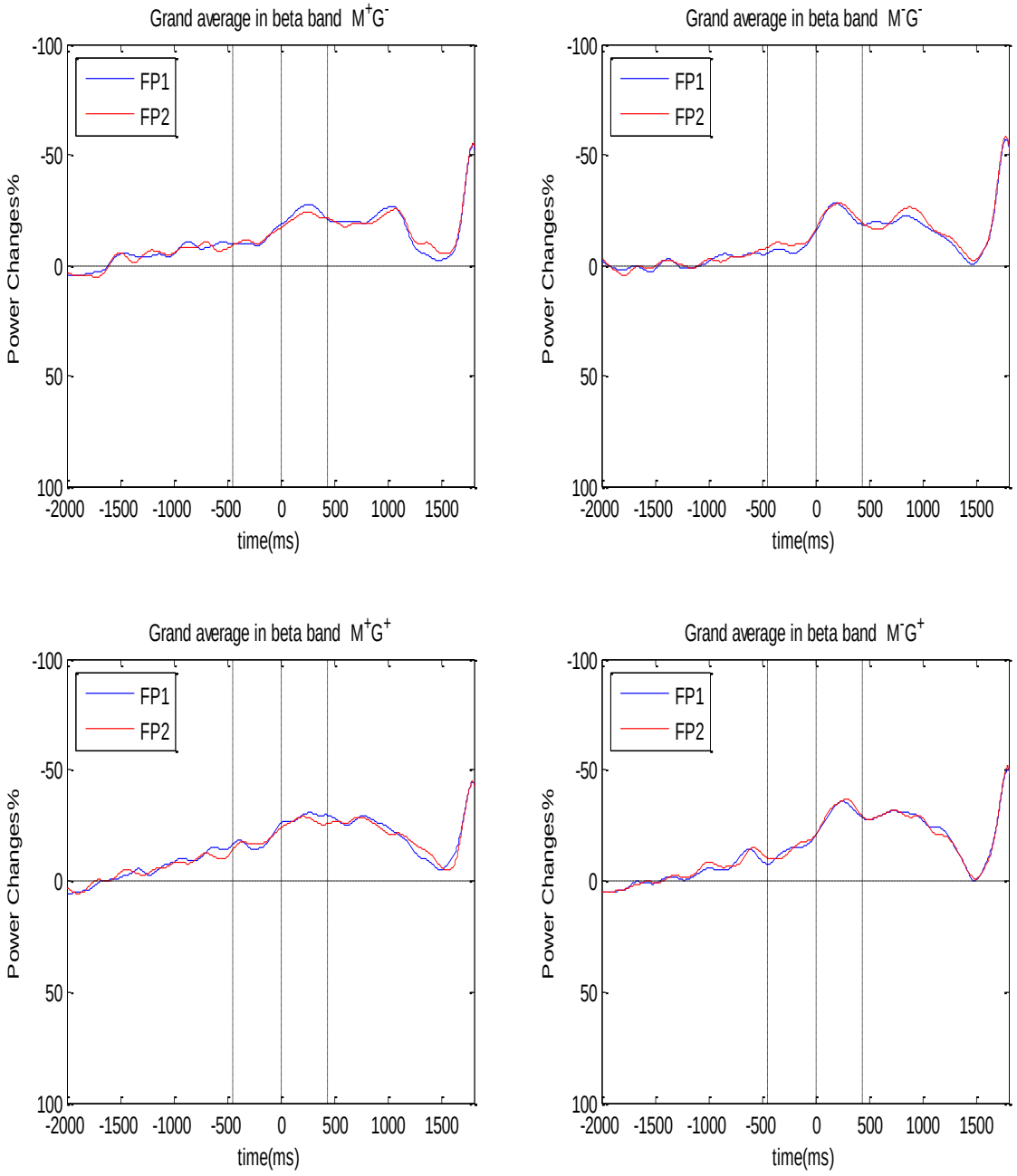

Figure 3.3 Grand average time-courses beta ERD at electrodes FP1 (blue line) and FP2 (red line). Four conditions (M^+G^-, M^-G^-, M^+G^+ and M^-G^+) are shown separately. Time 0 indicates movement onset and the first dash line which is before the 0ms indicated the 'move' cue and the last dash line represents the movement offset. An upward deflection indicates power decrease (ERD).

3.4 Grand Averaged ERS/ERD Comparisons between Hemispheres

Typical time-course of ERD during the right index finger flexion under four testing conditions (M^+G^-, M^-G^-, M^+G^+ and M^-G^+) are shown in Figure 3.4.1, Figure 3.4.2 and Figure 3.4.3. The contralateral cortex ERD activities were shown on the left side and the ipsilateral cortex ERD activity is shown on the right side.

A three-way RM ANOVA (loc (2 levels: C3-L, C4-R); Feedback (2 levels: mirror, no-mirror) and Goal (2 levels: goal, no-goal)) was conducted to explore the impact of mirror visual feedback (MVF) and movement goal on activity in bilateral primary motor cortex (left- and right-M1), as measured by beta ERD. 16 subjects participated in each condition. The significance level for all statistical analyses was set at $p<0.05$ (Table 2).

For the contralateral motor cortex (channel C3), the similar activity pattern but different ERD magnitudes can be observed in the preparation and execution phases. First, for the mirror groups' comparison the beta ERD magnitude of M^+G^- condition was larger than the M^+G^+ condition ones; and the ERD magnitude of M^-G^- condition was larger than the M^+G^- condition during the preparation and execution phases. Secondly, for the movement goal groups' comparison, the ERD magnitude of M^-G^- condition was lower than the M^-G^+ condition ones; and the ERD magnitude of M^+G^- condition was lower than the M^+G^+ condition ones. In brief, both mirror conditions showed lower ERD magnitude than the no-mirror conditions and both goal conditions showed larger ERD magnitudes than no-goal conditions. For the ipsilateral primary motor cortex (channel C4), the similar ERD as contralateral motor cortex. In addition, the ERD magnitudes at electrodes C3 and C4 reached the maximal values in the execution phase.

Statistical results indicated that the mirror effect (Feedback, $F(1, 15) = 18.05$, $p < 0.001$) is significant in the execution phase. The location (C3 and C4 electrodes) and feedback (mirror and no-mirror) interaction are both significant in preparation and execution phases (Preparation: $F(1, 15) = 22.03$, $p < 0.001$; Execution: $F(1, 15) = 12.58$, $p < 0.001$)). In Figure 3.4.4 and Figure 3.4.5, the ERD magnitude difference between left and right hemispheres in no-mirror conditions decreased when mirror was presented to subjects in preparation and execution phases.

Next, alpha ERD occurred after 'move' cue over bilateral parietal cortex for four conditions. Most interesting phenomenon showed at the ipsilateral parietal cortex (channel P4). For M^-G^- and M^+G^- conditions, the similar alpha ERD can be observed during preparation and execution phases. Same alpha ERD activity pattern can also be observed in M^-G^+ and M^+G^+ conditions as well. However, the differences between goal and no-goal conditions (M^+G^+ vs. M^+G^-; M^-G^+ vs. M^-G^-) were pronounced. The magnitudes of goal conditions were always lower than the no-goal conditions. Finally, as to the control sites plot (electrodes FP1 and FP2), Figure 3.4.3 showed similar ERD magnitudes over time and few difference among conditions. A three-way RM ANOVA (loc (2 levels: P3-L, P4-R); Feedback (2 levels: mirror, no-mirror) and Goal (2 levels: goal, no-goal)) was conducted to explore the impact of mirror visual feedback (MVF) and movement goal on activity in bilateral parietal cortex, as measured by alpha ERD. 16 subjects participated in each condition. The significance level for all statistical analyses was set at $p<0.05$ (Table 3). The statistical results indicated a significant goal effect in preparation and execution phases (Preparation: $F(1, 15) = 10.67$, $p = 0.001$; Execution: F

(1, 15) = 9.19, p = 0.003)). In Figure 3.4.6 and Figure 3.4.7, the alpha ERD magnitudes decreased when the movement goal was presented to subjects.

A B

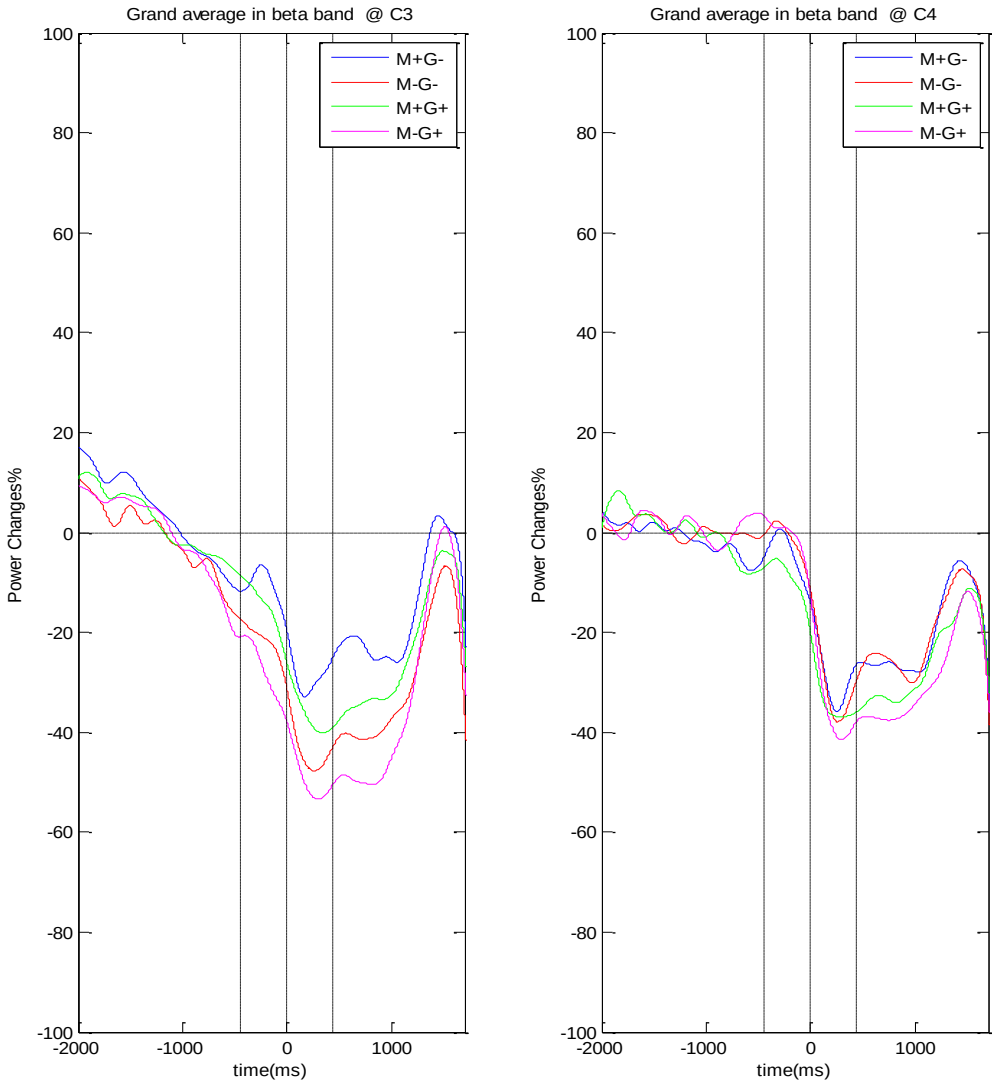

Figure 3.4.1 Averaged beta-band ERD comparisons over bilateral motor cortex. (A) The ERS/ERD activities across four conditions at the contralateral cortex (electrode C3). (B) The ERS/ERD activities across four conditions at the ipsilateral cortex (electrode C4). Three vertical dash lines represent move cue, move onset and move offset, respectively.

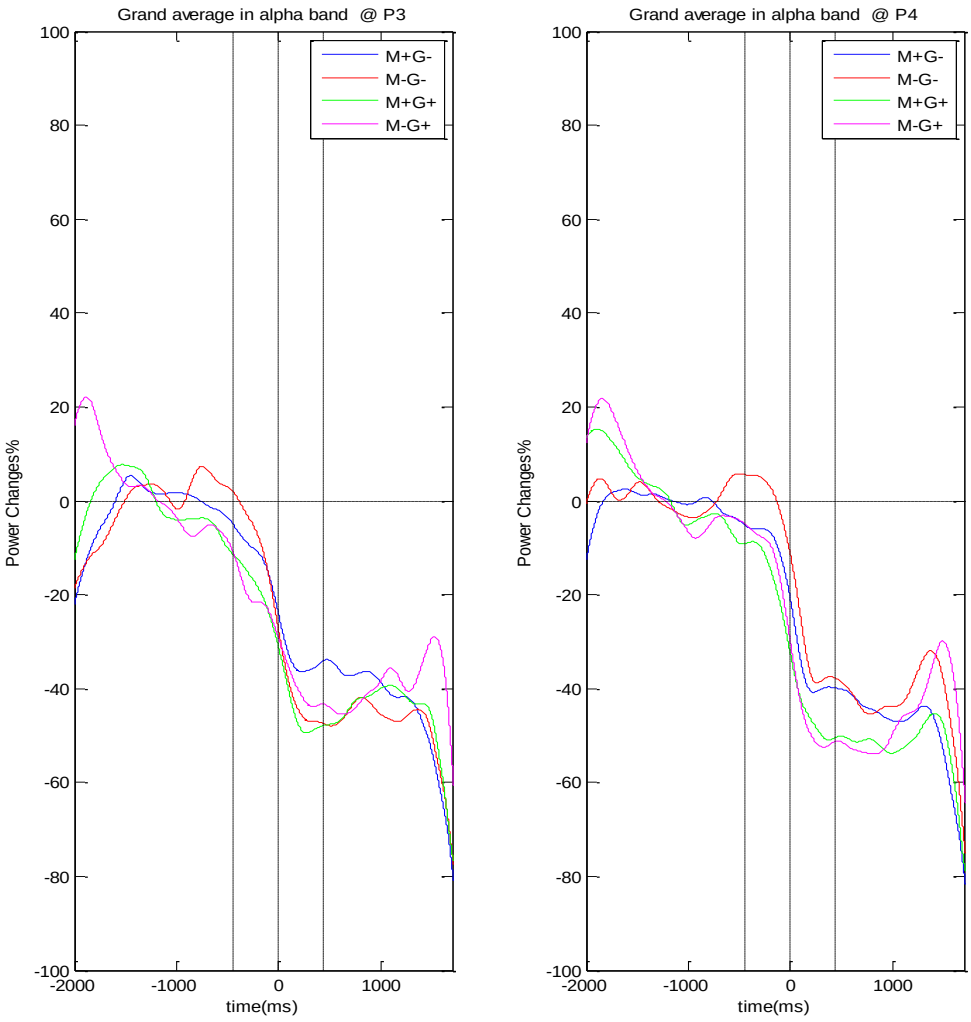

A B

Figure 3.4.2 Averaged alpha-band ERD comparisons over bilateral parietal cortex. (A) The ERS/ERD activities across four conditions at the contralateral cortex (electrode P3). (B) The ERS/ERD activities across four conditions at the ipsilateral cortex (electrode P4). Three vertical dash lines represent move cue, move onset and move offset, respectively.

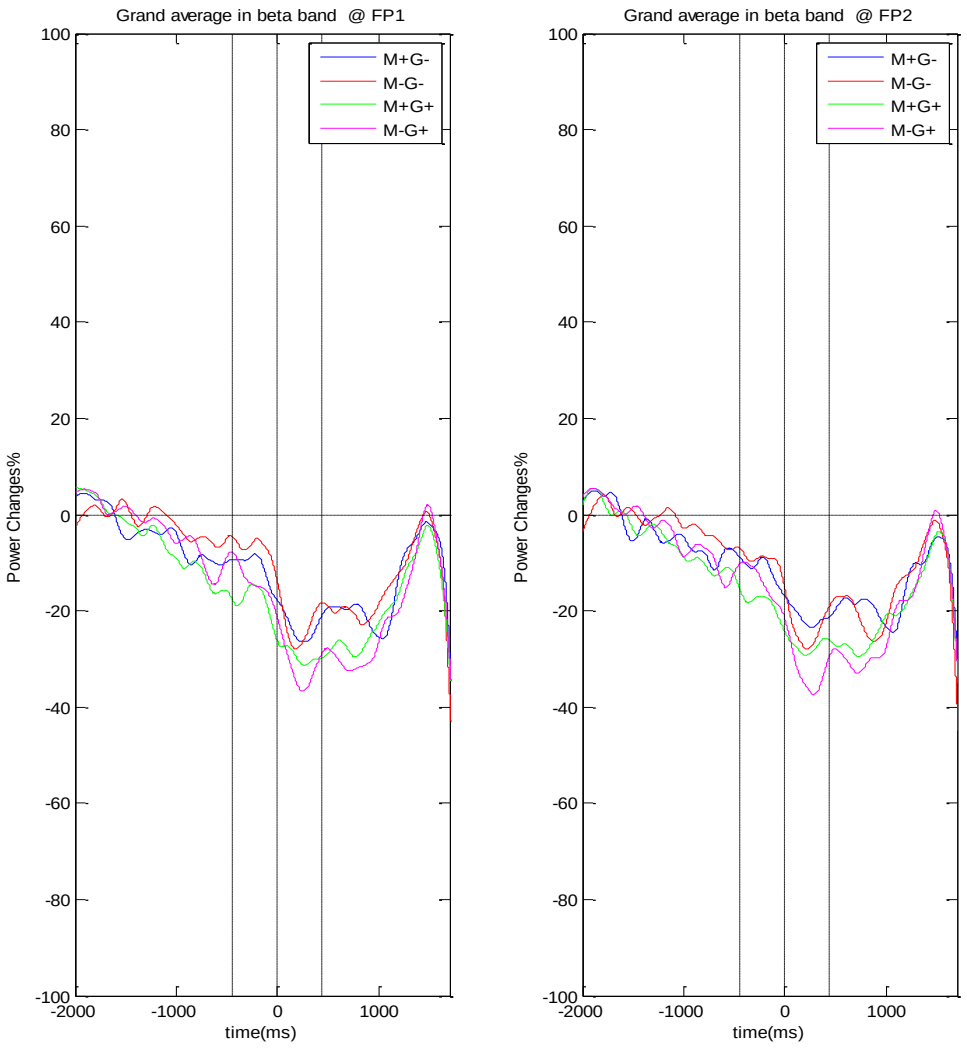

A B

Figure 3.4.3 Averaged beta-band ERD comparisons over control sites. (A) The ERS/ERD activities across four conditions at the contralateral cortex (electrode FP1). (B) The ERS/ERD activities across four conditions at the ipsilateral cortex (electrode FP2). Three vertical dash lines represent move cue, move onset and move offset, respectively.

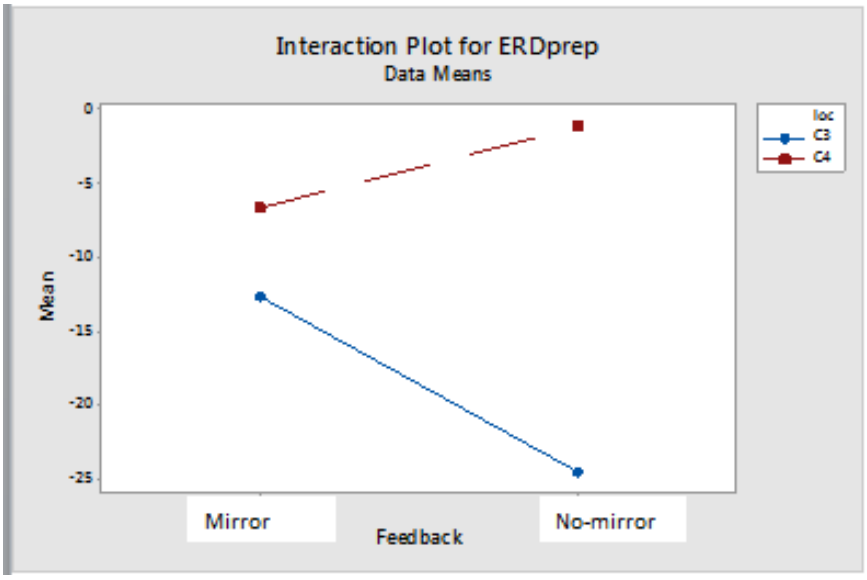

Figure 3.4.4 Interaction plot for mean beta ERD during preparation phase. Blue dots present mean beta ERD magnitudes at C3 electrode for mirror and no-mirror conditions. Red dots present mean beta ERD magnitudes at C4 electrode for mirror and no-mirror conditions. Abbreviations: prep—preparation.

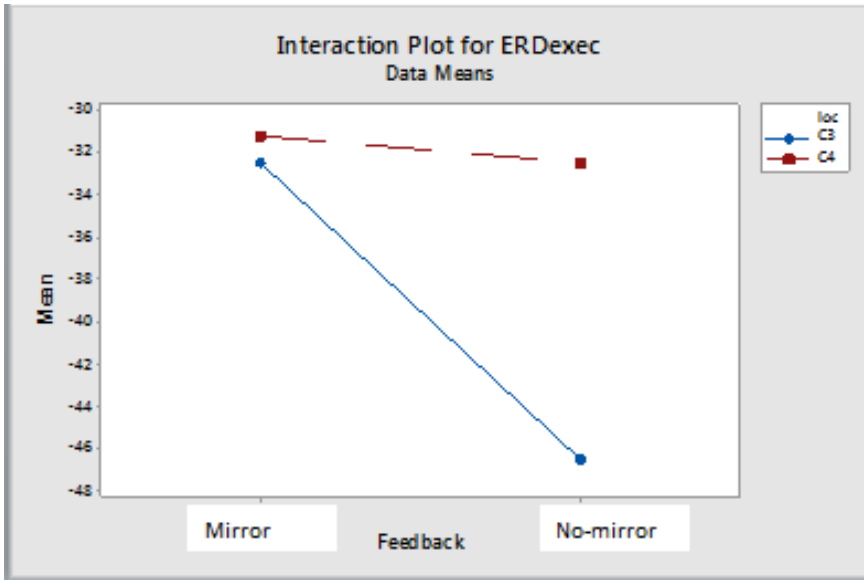

Figure 3.4.5 Interaction plot for mean beta ERD during execution phase. Blue dots present mean beta ERD magnitudes at C3 electrode for mirror and no-mirror conditions. Red dots present mean beta ERD magnitudes at C4 electrode for mirror and no-mirror conditions. Abbreviations: exec—execution.

Table 3.1 Main effects and interactions stemming from three-way ANOVA (loc (2 levels: C3-L, C4-R); Feedback (2 levels: mirror, no-mirror) and Goal (2 levels: goal, no-goal)) on mean beta ERD magnitudes in preparation and execution phases.

Preparation phase		
Source	F-value	P-value
Subjs	6.09	0.000
Loc	62.35	0.000
Feedback	2.95	0.089
Goal	3.36	0.070
Loc*Feedback	22.03	0.000
Loc*Goal	0.61	0.435
Feedback * Goal	0.26	0.614
loc*Feedback*Goal	0.99	0.322

Execution phase		
Source	F-value	P-value
Subjs	6.85	0.000
Loc	18.31	0.000
Feedback	18.05	0.000
Goal	9.51	0.003
Loc*Feedback	12.58	0.001
Loc*Goal	0.14	0.711
Feedback * Goal	0.18	0.675
loc*Feedback*Goal	0.02	0.893

Abbreviations: subjs—subjects, loc—location.

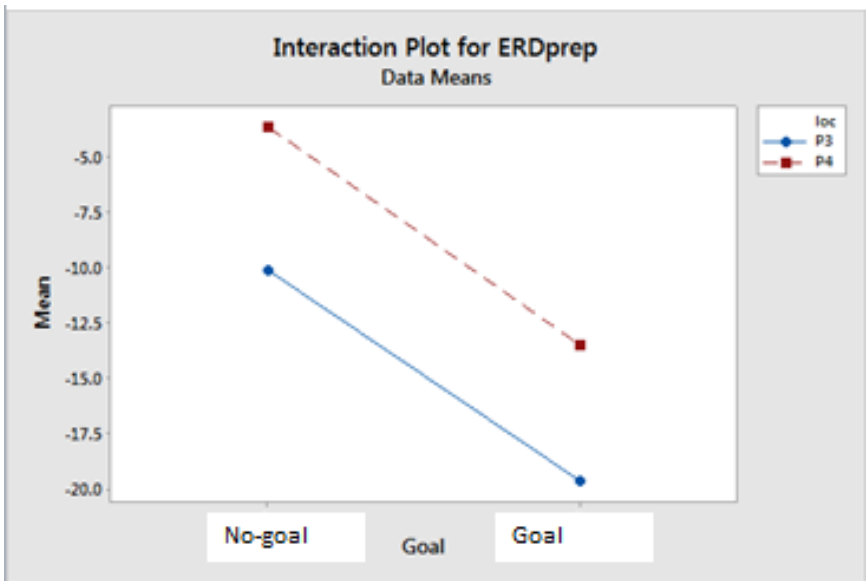

Figure 3.4.6 Interaction plot for mean alpha ERD during preparation phase. Blue dots present mean ERD magnitudes at C3 electrode for mirror and no-mirror conditions. Red dots present mean ERD magnitudes at C3 electrode for mirror and no-mirror conditions. Abbreviations: prep—preparation.

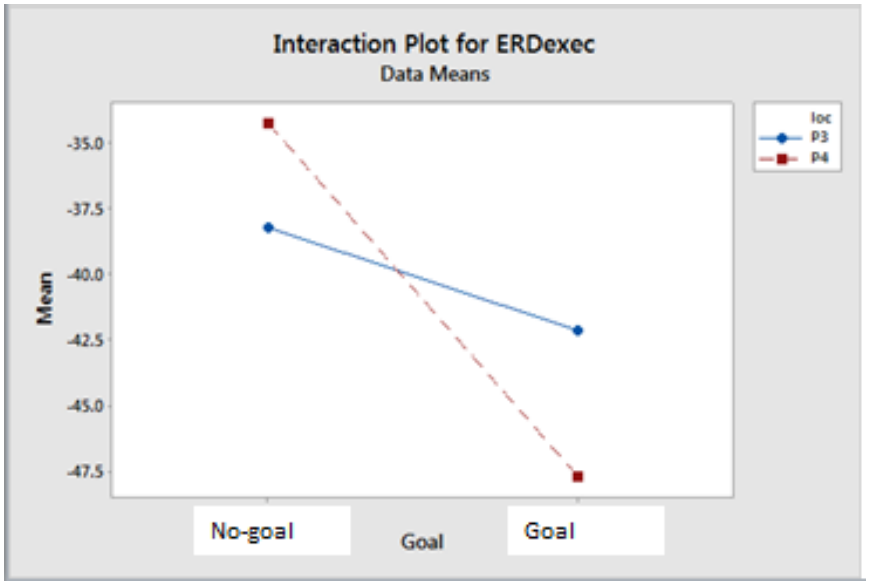

Figure 3.4.7 Interaction plot for mean alpha ERD during execution phase. Blue dots present mean alpha ERD magnitudes at P3 electrode for goal and no-goal conditions. Red dots present mean alpha ERD magnitudes at P4 electrode for goal and no-goal conditions. Abbreviations: exec—execution.

Table 3.2 Main effects and interactions stemming from three-way ANOVA (loc (2 levels: P3-L, P4-R); Feedback (2 levels: mirror, no-mirror) and Goal (2 levels: goal, no-goal)) on mean alpha ERD magnitudes in preparation and execution phases.

Preparation phase		
Source	F-value	P-value
Subjs	10.16	0.000
Loc	4.48	0.037
Feedback	1.67	0.199
Goal	10.67	0.001
Loc*Feedback	1.10	0.298
Loc*Goal	0.00	0.952
Feedback * Goal	0.92	0.339
loc*Feedback*Goal	0.01	0.931

Execution phase		
Source	F-value	P-value
Subjs	12.75	0.000
Loc	0.08	0.784
Feedback	0.05	0.821
Goal	9.19	0.003
Loc*Feedback	0.63	0.430
Loc*Goal	2.78	0.099
Feedback * Goal	0.73	0.396
loc*Feedback*Goal	2.47	0.119

Abbreviations: subjs—subjects, loc—location.

3.5 Sum of Squared Error (SSE)

To explore the inter-hemispheric activation (ERD) difference, the sum of squared error (SSE) was calculated under different movement phases for three paired channels (C3 – C4, P3 – P4, FP1 – FP2) in each condition. The results were shown below (Figure 3.5). It should be noted that the whole experiment contains two movements, flexion and extension, which means the post-movement phase is only for the post-flexion phase but it also contained the cortical activity. Since the purpose was to identify significant differences between conditions (mirror, no-mirror, goal and no-goal conditions), the independent two-sample t-test was used to assess the goal and mirror effects over bilateral primary motor cortex (Table 4), parietal cortex (Table 5) and control sites (Table 6).

In grand average SSE calculation for C3 – C4 electrode pair (Figure 3.5.A), no significant difference was illustrated between conditions both in the pre-movement and post-movement phases (Table 4). Then in the preparation phase, the SSE magnitude in $M^{+}G^{-}$ was greatly lower than that in $M^{-}G^{-}$ condition ($p < 0.05$). Also the SSE magnitude in $M^{+}G^{+}$ was much lower than $M^{-}G^{+}$ condition ones during the same phase ($p = 0.0277$). As for the execution phase, the same pattern can be observed ($M^{+}G^{-}$ vs. $M^{-}G^{-}$, $p < 0.05$; $M^{+}G^{+}$ vs. $M^{-}G^{+}$, $p < 0.05$). In other words, the no-mirror conditions ($M^{-}G^{-}$and $M^{-}G^{+}$) showed larger inter-hemispheric activation difference than mirror conditions ($M^{+}G^{-}$ and $M^{+}G^{+}$) in preparation and execution phases. Besides, no significant effect can be found between goal and non-goal conditions during preparation phase. In addition, no significant effect can be observed in pre-movement and post-movement phases.

In grand average SSE calculation for P3 – P4 electrode pair (Figure 3.5.B), during the pre-movement and post-movement phases, no significance can be observed. In the preparation and execution of movement phases, the pattern of SSE magnitudes distribution over all conditions was similar with the C3 – C4 electrode pair results, which SSE values in no-mirror conditions were larger than that in mirror conditions (M^-G^- vs. M^+G^-; M^-G^+ vs. M^+G^+). The significance only existed between M^+G^+ vs. M^-G^+ group ($p = 0.0118$) during preparation phase.

Finally, for the control sites, grand average SSE for FP1 – FP2 electrode pair was shown in Figure 3.5.C, the SSE magnitudes for all conditions and phases were no significant (Table 6).

A

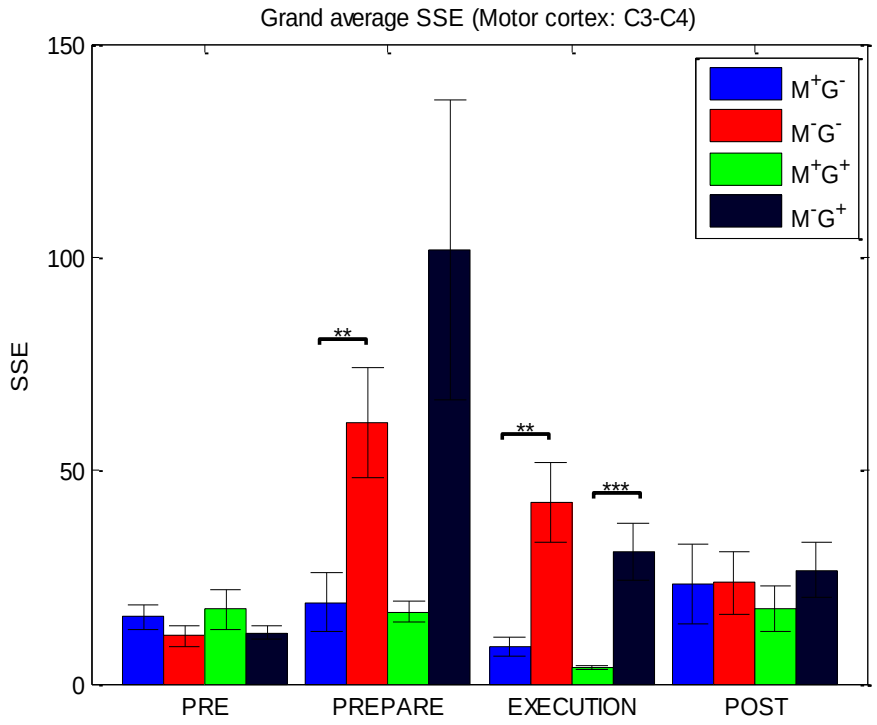
Grand average SSE (Motor cortex: C3-C4)
SSE
150
100
50
0
M+G-
M-G-
M+G+
M-G+
**
**
***
PRE
PREPARE
EXECUTION
POST

B

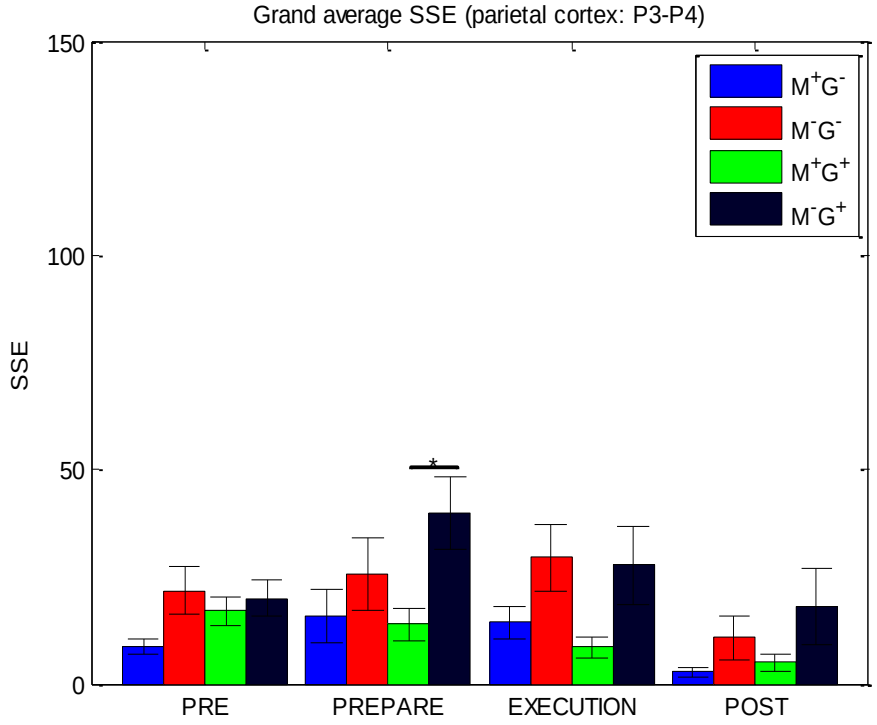
Grand average SSE (parietal cortex: P3-P4)
SSE
150
100
50
0
M+G-
M-G-
M+G+
M-G+
*
PRE
PREPARE
EXECUTION
POST

C

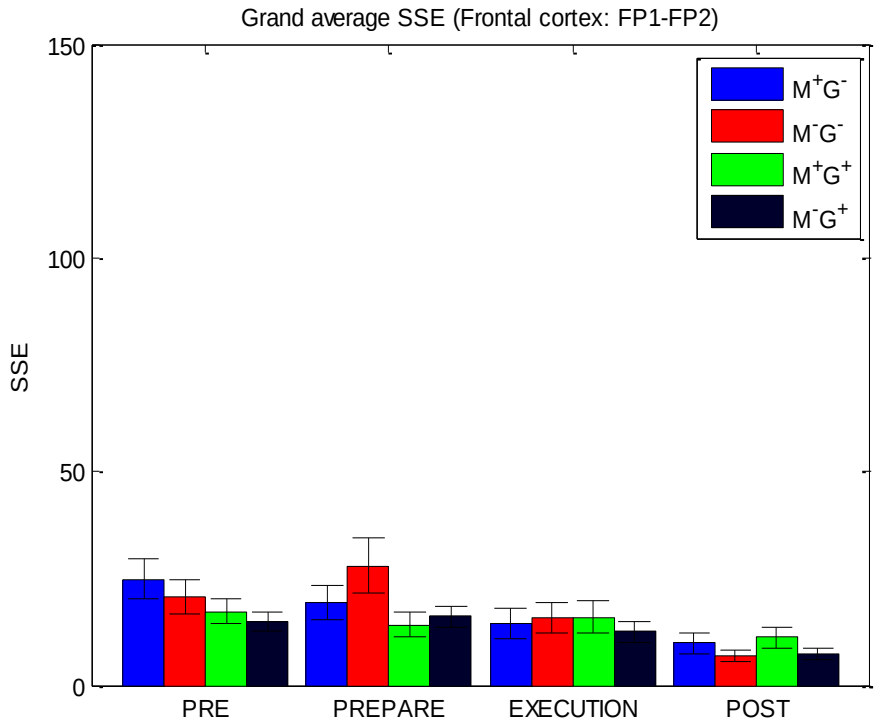

Figure 3.5 Grand averaged sum of square error (SSE) for three electrode pairs in different movement phases. (A) SSE for C3 – C4 electrode pair in the four conditions (M^+G^-, M^-G^-, M^+G^+ and M^-G^+) during four phases (pre-movement phase, preparation phase, execution of movement phase and post-movement phase). (B) SSE for P3 – P4 electrode pair in the four conditions and four phases. (C) SSE for FP1 – FP2 electrode pair in the four conditions and four phases. Electrodes FP1 and FP2 were considered as control sites. Blue bar represents M^+G^- condition; red bar represents M^-G^- condition; green bar represents M^+G^+ condition; black bar represents M^-G^+ condition, respectively. Error bar represented the standard error of the mean. Significant differences between bars were indicated by asterisks. * represents p<=0.05, ** represents p<=0.01, ***represents p<=0.001.

Table 3.3 Two sample t-test on C3-C4 SSE magnitudes between conditions in preparation and execution phases

	Pre	Prep	Exec	Post
M^+G^- vs. M^-G^-	0.2521	0.0093	0.0022	0.9696
M^+G^+ vs. M^-G^+	0.2757	0.0277	0.0007	0.2924
M^+G^- vs. M^+G^+	0.7369	0.7601	0.0374	0.6150
M^-G^- vs. M^-G^+	0.7999	0.3039	0.3513	0.7666

Abbreviations: Prep—preparation, Exec—execution.

Table 3.4 Two sample t-test on P3-P4 SSE magnitudes between conditions in preparation and execution phases

	Pre	Prep	Exec	Post
M^+G^- vs. M^-G^-	0.0706	0.3608	0.1032	0.1496
M^+G^+ vs. M^-G^+	0.5887	0.0118	0.0551	0.1879
M^+G^- vs. M^+G^+	0.0772	0.8021	0.2183	0.3697
M^-G^- vs. M^-G^+	0.8080	0.2704	0.8860	0.5078

Abbreviations: Prep—preparation, Exec—execution.

Table 3.5 Two sample t-test on FP1-FP2 SSE magnitudes between conditions in preparation and execution phases

	Pre	Prep	Exec	Post
M^+G^- vs. M^-G^-	0.5139	0.2853	0.8177	0.3193
M^+G^+ vs. M^-G^+	0.5031	0.6357	0.4903	0.2013
M^+G^- vs. M^+G^+	0.1913	0.3290	0.7958	0.7151
M^-G^- vs. M^-G^+	0.2315	0.1062	0.4921	0.8367

Abbreviations: Prep—preparation, Exec—execution.

It should be noted that the subjects in this MVF experiments were tested in two different orders (Table 1). For the first testing group (11 subjects), the mirror sessions (M^+G^- and M^+G^+) and the no-mirror sessions (M^-G^- and M^-G^+) were tested in separate days. The no-goal condition was always tested prior to goal condition. But for the second group (5 subjects), the no-goal sessions (M^+G^- and M^-G^-) and the goal sessions (M^+G^+ and M^-G^+) were tested in separate days. The Figure 3.6 illustrated that the different orders of testing can really impact the cortical activity (alpha oscillations in parietal cortex). The two sample t-test was used to assess the order influence.

In detail, in the first testing group (11 subjects group, Figure 3.6.A), the comparison between goal conditions illustrated that the SSE magnitude in M^-G^+ condition was much higher than that in M^+G^+ condition during preparation and execution phases. But only the preparation phase showed the significant effect (M^+G^+ vs. M^-G^+, $p < 0.05$). The comparison between no-goal conditions (M^-G^- vs. M^+G^-) didn't show any significant SSE difference in these two phases. In addition, in the two no-mirror conditions, we found out the goal effect (M^-G^- vs. M^-G^+, $p < 0.05$) only in the preparation phase. As for the two mirror conditions (M^+G^- and M^+G^+), few significance can be found out. For the second testing group (5 subjects group, Figure 3.6.B), the comparison between no-goal conditions showed a strong significance (M^+G^- vs. M^-G^-, $p < 0.05$). Even though in the execution phase the SSE magnitudes of no-mirror conditions were higher than mirror conditions (M^-G^- vs. M^+G^-, M^-G^+ vs. M^+G^+), no significance can be found out (Table 7). During the pre-movement phase, both testing groups didn't show any significance (Table 8), which can indicate that the pre-movement significance effect of the 16 subjects group was random.

A

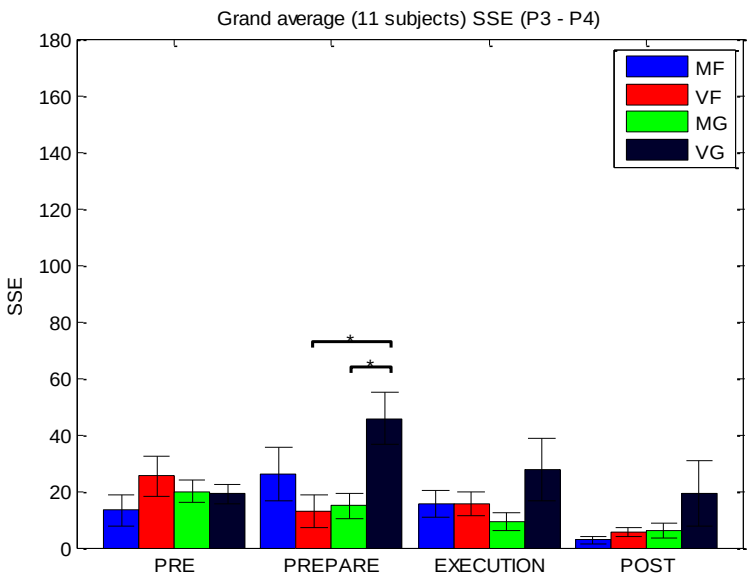

B

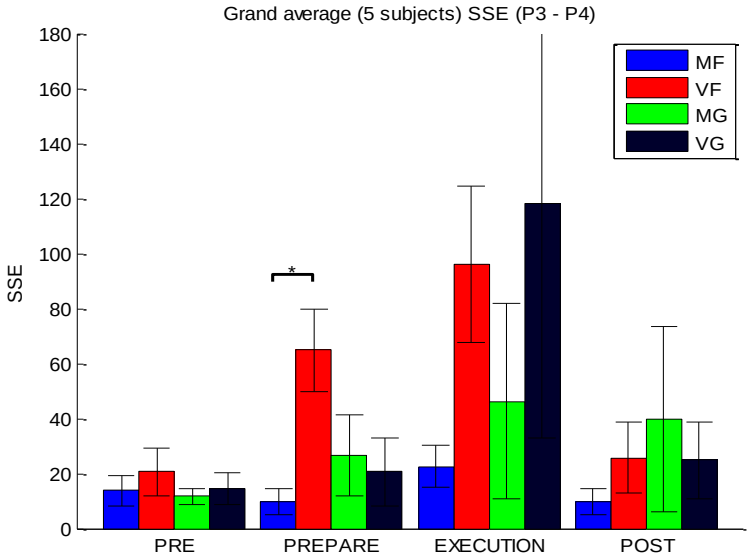

Figure 3.6 The effect of the order of experiments. (A) in the 11 subjects group, the mirror sessions (M^+G^- and M^+G^+) and the veridical sessions (M^-G^- and M^-G^+) were tested in different days. The free condition was always tested first. (B) In the 5 subjects group, the free sessions (M^+G^- and M^-G^-) and the goal sessions (M^+G^+ and M^-G^+) were tested in separate days. Blue bar represents M^+G^- condition; red bar represents M^-G^- condition; green bar represents M^+G^+ condition; black bar represents M^-G^+ condition, respectively. Error bar represented the standard error of the mean. Significant differences between bars were indicated by asterisks. * = $p<0.05$.

Table 3.6 Two sample t-test on P3-P4 SSE magnitudes (11 subjects) between conditions on preparation and execution of movement phases

	Pre	Prep	Exec	Post
M^+G^- vs. M^-G^-	0.2122	0.2703	0.9831	0.2481
M^+G^+ vs. M^-G^+	0.9046	0.0095	0.1418	0.3148
M^+G^- vs. M^+G^+	0.3589	0.3199	0.2945	0.2870
M^-G^- vs. M^-G^+	0.4667	0.0089	0.3473	0.2861

Abbreviations: Prep—preparation, Exec—execution.

Table 3.7 Two sample t-test on P3-P4 SSE magnitudes (5 subjects) between conditions on preparation and execution of movement phases

	Pre	Prep	Exec	Post
M^+G^- vs. M^-G^-	0.5698	0.0143	0.0549	0.3372
M^+G^+ vs. M^-G^+	0.7128	0.7836	0.5059	0.7253
M^+G^- vs. M^+G^+	0.7882	0.3496	0.5742	0.4573
M^-G^- vs. M^-G^+	0.6116	0.0788	0.8308	0.9687

Abbreviations: Prep—preparation, Exec—execution.

3.6 Global Field Power (GFP) and Scalp Maps

To analyze the cortical responses to the specific conditions, scalp maps of the cortical activity occurring during first three peaks in the global field power (GFP) were visualized. Figure 3.7 showed that conditions had similar GFP oscillations and right index finger flexion produced the largest deflections in M^-G^+ condition during execution of movement phase. In addition, three peaks of GFP can be observed, where the first peak was in the preparation phase and the resting two peaks located in the movement execution phase. And more deflections can be observed in the two goal conditions (M^-G^+ and M^+G^+) than the free conditions (M^-G^- and M^+G^-) at the second peak which was close to move onset. Topographies (Figure 3.8) corresponded to peaks of GFP were displayed. The first column indicated the cortical activity in the preparation phase and the following two columns were the cortical activity during movement execution phase, respectively. From the topographic results, the frontal regions were activated during preparation phase. Very similar spatial activation patterns were obtained from M^+G^- and M^-G^- conditions. Scalp map of M^+G^+ condition showed a symmetric scalp map, while, scalp map of M^-G^+ condition showed a more lateralized potential distribution. The second scalp maps indicated that the central and frontal regions worked together to execute the movement, but more cortical activity can be observed in the parietal cortex in the two goal conditions (M^-G^+ and M^+G^+) rather than the two free conditions (M^-G^- and M^+G^-). Moreover, the latency of M^+G^+ condition in the second peak appeared earlier than other three conditions. Finally, the parietal regions were activated in all conditions.

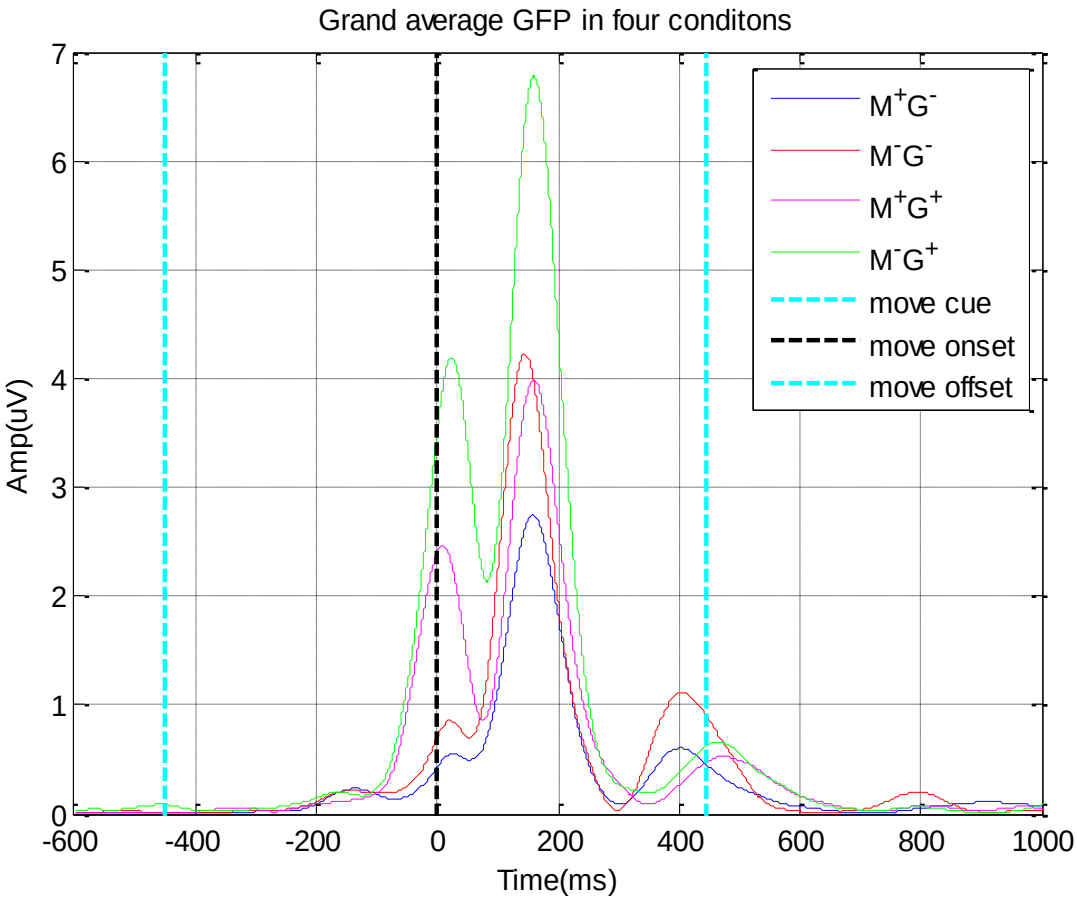

Figure 3.7 Global field power (GFP) comparison. Four conditions GFP were plotted together to determine and compare the latency of each peak. Three vertical dash lines represent move cue, move onset and move offset.

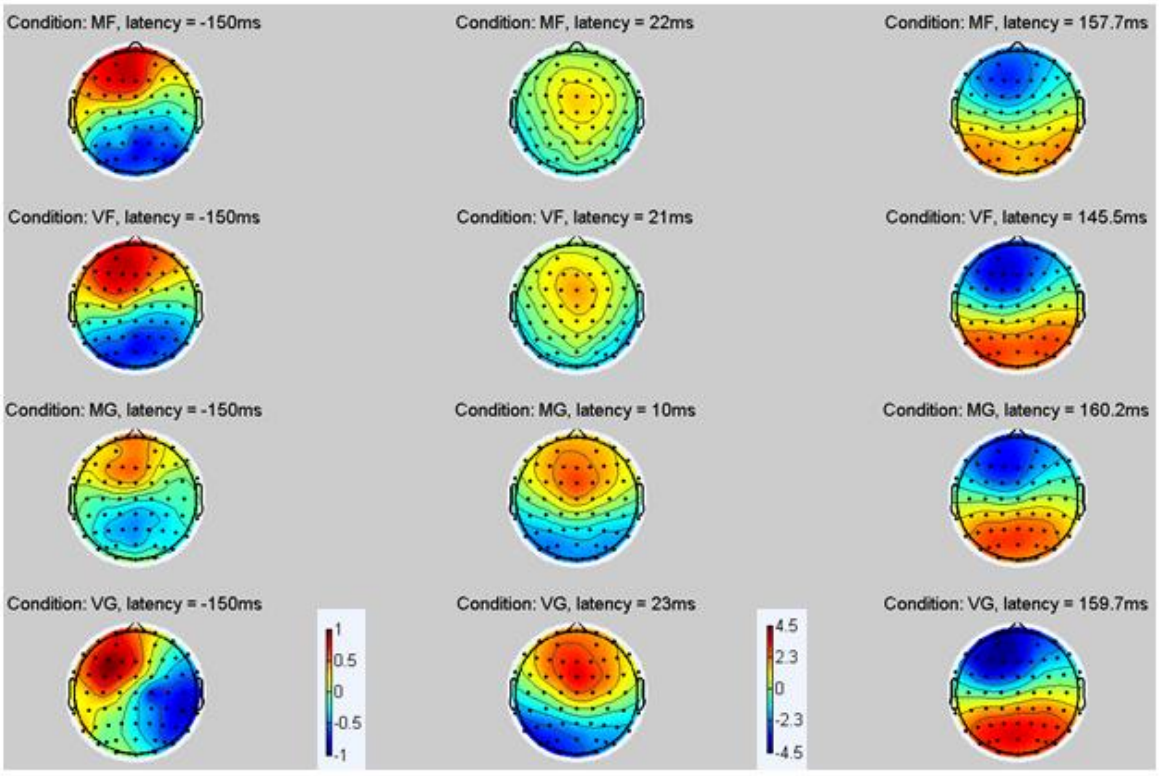

Figure 3.8 Topographic maps. Each row represented topographies of one condition which occurred in the order of three peaks in the GFP. Each column represented potential distribution if brain activity which occurred among different conditions but similar latency. Component latency was determined by each peak in GFP. Time 0ms represented movement onset. The second and third columns have the same color bar scale. Numbers in color bar scales indicate minimal (blue) and maximal (red) values (in μV) within the three plots. (V = No-mirror; M = Mirror; F = No-goal; G = Goal)

The movement-relate scalp maps were presented in Figure 3.10, each condition contains six scalp maps whose latency ranged from 70ms to 90ms after movement onset and the interval was 4ms. For the $M^{+}G^{+}$ and $M^{-}G^{+}$ conditions, a strong dipole-like scalp map can be observed ($M^{+}G^{+}$ at 82ms; $M^{-}G^{+}$ at 86ms). For the $M^{+}G^{-}$ and $M^{-}G^{-}$ conditions, a weak dipole-like scalp map can be observed ($M^{+}G^{-}$ at 78ms; $M^{-}G^{-}$ at 78ms).

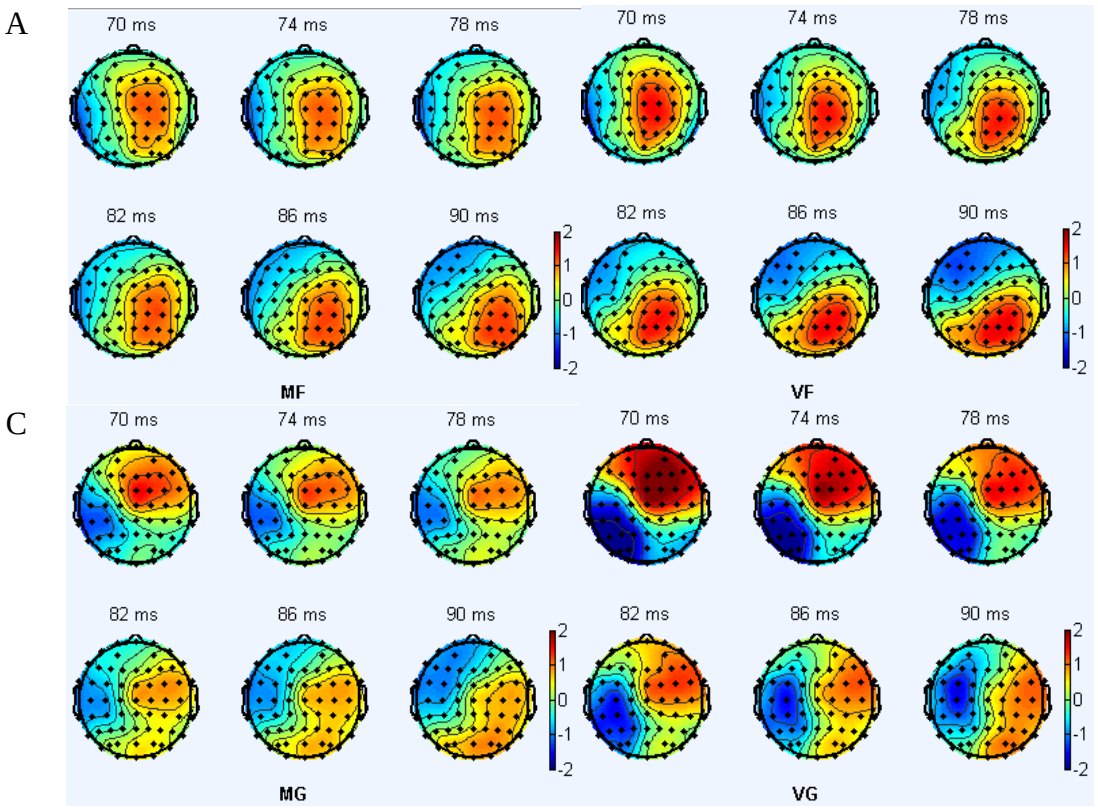

Figure 3.9 Scalp potential distributions in four conditions. The scalp distributions are based on a right hand movement data. 0ms represents the movement onset. (V = No-mirror; M = Mirror; F = No-goal; G = Goal)

CHAPTER 4

DISCUSSION

In this study, a novel VR training system based on digital technology was developed to determine the effects of mirror (MVF) and movement goal on cortical activation, rather than using the traditional physical mirror box. Sixteen healthy right-handed subjects were tested in four testing conditions ($M^{+}G^{-}$, $M^{-}G^{-}$, $M^{+}G^{+}$ and $M^{-}G^{+}$) and their cortical activations were recorded using high-intensity EEG technique at the same time. One of the measurements for the cortical activation called event-related desynchronization (ERD) which reflected the neural activity changes over primary motor cortex and parietal cortex.

After seeing the move cue, alpha/beta band power decreased on bilateral motor cortex, parietal cortex and prefrontal cortex (control sites). This activity pattern was found in all testing conditions during index finger flexion. The ERD calculation formula pointed out the magnitude of ERD can reflect the percentage of power relative to the reference and therefore it depends on the amount of rhythmic activity or neural networks in the movement interval. Previous studies concluded that certain events can block or desynchronize the ongoing beta/alpha activity [10, 31]. In short, the magnitude of ERD represents the extent and degree of desynchronization. In our results, the alpha/beta ERD magnitudes decreased gradually and got the maximum in the execution phase for all testing conditions and all three paired channels. This means the neural networks or elements desynchronized gradually. In detail, beta power changes (beta ERD) in motor cortex are observed during movement execution. This means the neural elements located

around the motor cortex were desynchronized by hand movements. Alpha power changes (alpha ERD) in parietal cortex are observed during goal-directed movements. This represents that the neural elements located around the parietal cortex were desynchronized by the presence of goal. This is in agreement with the previous studies [10, 31]. For the beta-band ERD, a power rebound (which magnitude went back to 0%) appeared during post-movement phase for channel C3 and C4, which means that active neurons at the primary motor cortex is resetting to resting state for preparing the next movement. However, in channel P3 and P4, we didn't observe this resetting phenomenon. The reason may be that a 'return' cue following the 'move' cue can also induced the alpha band oscillation on parietal cortex, thus the brain didn't have enough time to return the resting status.

In summary, alpha and beta ERD demonstrated that the neural elements which were around the motor cortex and parietal cortex can be activated in testing conditions ($M^{+}G^{-}$, $M^{-}G^{-}$, $M^{+}G^{+}$ and $M^{-}G^{+}$) and the excitation levels were different from conditions. Since we used the VR system to investigate the mirror (MVF) and goal effects, the similar cortical activity (alpha and beta ERD) proved that the VR system is as useful as the traditional 'mirror box' [10, 33]. Further, the different desynchronization levels among conditions may due to the two factors of experiments: mirror and goal.

4.1. Beta ERD in Primary Motor Cortex

One of the main findings in this study was the significant effect of mirror (or MVF). This effect was reflected by the beta ERD rhythm over primary motor cortex. The great inter-hemispheric activation difference at primary motor cortex (beta ERD at electrodes C3 vs. C4) in no-mirror conditions reduced when the mirror was provided. In

other words, it suggested that asymmetry in hemispheric activation will be reduced by mirror visual feedback (MVF). This is in agreement with one of previous studies on ERD/ERS patterns obtained with unilateral wrist extension movements performed with and without mirror [30].

Which hemisphere is more active by mirror visual feedback stimulus? Recently, many studies using different methods to explore the mirror visual feedback (MVF) effect and found out a lot of interesting results. Since the non-impaired hemisphere also has an ipsilateral control pathway to the impaired limb, recruitment of the ipsilateral motor pathways during movement of the active hand has been considered by a recent review article as part of the MVF effects on motor recovery [34]. However, separate hemispheric beta ERD analyses (M^-G^- vs. M^+G^-; M^-G^+ vs. M^+G^+) in our study showed that the mirror visual feedback (MVF) significantly reduced ERD magnitude in the contralateral- (left-) instead of ipsilateral (right-) hemisphere during hand movements. In other words, the mirror didn't significantly affect ipsilateral primary motor pathways during movements, whatever in goal conditions (M^+G^+ vs. M^-G^+) or no-goal conditions (M^+G^- vs. M^-G^-). One of possible interpretations is that the recruitment of ipsilateral motor pathways might play a less important role in the mirror visual feedback (MVF) effects on healthy subjects, because the previous study investigated the mirror visual feedback (MVF) effect on patients after stroke. Another explication is due to the analysis methods' difference because in this study we used ERD to explore the cortical activity which is more specific than the original event-related potentials (ERPs) or other neural imaging methods, such as functional MRI. However, previous paper found that MVF-induced attenuation of ERD magnitude play an important role in the hemisphere which was contralateral to the

moving right hand for a group of health subjects [30]. Our beta ERD is in line with their conclusion. Moreover, a similar mirror visual feedback (MVF) effects were obtained from a TMS study [31]. In that study, it showed increased intra-cortical inhibition in the left hemisphere following four days of MVF training using the right hand. However, another TMS study also found out a concomitant increase in cortical excitability in the hemisphere ipsilateral to the moving hand [38]. This may be due to the involvement of different neuronal populations between TMS and VR-induced movements. TMS directly stimulated the cortical-spinal neurons, but neurons which were located around primary motor cortex were activated by VR-induced movements. Thus, in the view of the explanations from TMS study, the mirror-induced beta ERD attenuation in the hemisphere contralateral to the moving hand during right index finger movements was likely to reflect increased intra-cortical inhibition. In addition to the hemispheric asymmetry investigation, the beta ERD appeared at ipsilateral (right) cortex in $M^{+}G^{+}$ condition was earlier than other three conditions, and its ERD magnitude was also a little larger than other three conditions. This means the combination of mirror visual feedback (MVF) and movement goal can evoke early neurons activation at ipsilateral cortex for preparing the movements. The explanation might be that mirror-goal stimulus is a mean to facilitate the interconnection between action execution and action observation. In brief, neural elements or networks are desynchronized faster and more strongly in the ipsilateral (right) primary motor cortex during movement preparation phase only when the movement goal provided in the mirror side.

Next, which phase was mainly influenced by mirror visual feedback (MVF) stimulus? Experimental diagram introduced four phases: pre-movement phase;

preparation phase; execution phase and post-movement phase. The comparison between SSE magnitudes of mirror and no-mirror conditions (M^-G^- vs. M^+G^-; M^-G^+ vs. M^+G^+) indicated that the asymmetry in hemispheric activation which was reduced by mirror visual feedback (MVF) only occurred in preparation and execution phases. This significant phenomenon can also be observed in Figures 3.4.5 and 3.4.6. The attenuation of inter-hemispheric asymmetry may be due to movement observation and movement execution share the same neural mechanism.

In addition, the goal effect also observed in beta ERD results. In our results, movement goal can increase the contralateral (left) ERD magnitudes during preparation and execution of movements phase. This suggested that the goal can extend and increase the strength of the neural elements desynchronization on the contralateral (left) hemisphere. As to the inter-hemisphere activation difference (SSE), the significant effect of goal only occurred between M^+G^- and M^+G^+ conditions in the execution phase. Moreover, statistical results showed significant goal effect in the execution phase as well. This suggested that, in addition to mirror visual feedback (MVF) effect, the attenuation of cortical asymmetry can be enhanced by the presence of goal.

However, attenuation of inter-hemisphere activation difference induced by mirror visual feedback (MVF) might result from the data analysis mistake or environmental factors. This possibility can be excluded because the beta-ERD activation and its corresponding SSE magnitudes at the prefrontal cortex (control sites) didn't show any significance among conditions and phases (pre-movement phase; preparation phase; execution phase and post-movement phase). This represents the cortical activation changes are represented in the primary motor cortical region with respect to the mirror

effect, rather than with respect to commands to specific factors.

In summary, mirror visual feedback (MVF) can reduce of inter-hemispheric asymmetry. This attenuation occurred in the movement preparation and execution phases. One possible explanation is that the action observation and execution share the same neural mechanism, which means both would desynchronize the neural elements. This is likely called the intra-cortical inhibition [31]. But the movement goal can increase the cortical activation, and the reason might be that movement goal can increase the complexity and strength of movements. Moreover, in the mirror conditions (M^+G^- and M^+G^+); the presence of goal would greatly reduce the hemispheric asymmetry during execution of movement phase. However, no mirror-goal effect can be observed during movements.

4.2. Alpha ERD in Parietal Cortex

In addition to the investigation of mirror visual feedback (MVF) effect, another factor manipulated in this study is the movement goal. The cortical activation was analyzed since the alpha-band activity in parietal lobe is related to the cognitive mechanism and goal-directed movement planning [33]. The alpha-ERD results at parietal cortex showed distinct patterns between goal and non-goal conditions. The alpha ERD magnitudes at ipsilateral (right) parietal cortex significantly decreased when goal was presented to subjects. Previous studies also reported the same results which significantly lower power values for alpha band during observation of a precision grip (goal-directed movement) relative to those during observation of a simple hand extension (non-goal direct movement), and cortical dynamics during active movements and action observation share the common mechanisms [33]. There are two possible interpretations

of this phenomenon. The first one is that two different neuronal populations are involved, according to the presence of a goal or no goal, and that their activation induced a different level of desynchronization [37]. The other explanation is that the same neuronal populations for both type of movements, but the presence of a goal requires more complex processing, leading to a greater desynchronization [33]. The statistical results also indicated the significant goal effect in execution and preparation phases.

Next, the alpha SSE magnitude differences between no-goal conditions (M^+G^- vs. M^-G^-) in preparation and execution phases are obvious. The reason may be due to the order of experiments. In the first testing group, 11 subjects were tested in two mirror conditions (M^+G^+ and M^+G^-) and two no-mirror conditions (M^-G^- and M^-G^+) in separate days. The conditions which contain a goal were always tested followed condition which didn't have any goal. In the second group, 5 subjects were tested in two goal conditions (M^-G^+ and M^+G^+) and two no-goal conditions (M^-G^- and M^+G^-) in separate days. In the preparation and execution phases, the SSE magnitudes for M^+G^- and M^-G^- conditions in the first testing group were similar. But the significant higher SSE magnitude in M^-G^- condition comparing to M^+G^- condition can be observed in the second testing group, which can directly explain the pronounced differences between no-goal conditions (M^+G^- vs. M^-G^-) in preparation and execution phases for sixteen subjects averaging SSE results. This proved that the order of experiments can really impact the alpha-band ERD oscillations. Thus, the second testing groups were excluded for the following discussion.

In the preparation phase, the first testing group showed a significant goal effect in no-mirror conditions (M^-G^- vs. M^-G^+). Because SSE magnitude can work as an index of the hemispheric asymmetry, the higher SSE magnitude in M^-G^+ condition during

preparation phase suggested that goal can induce higher hemispheric asymmetry. This result is in agreement with the previous study [33] and the reason should be due to the goal effect. But this effect was attenuated in mirror conditions (M^+G^- vs. M^+G^+). This may suggest that the presence of goal wouldn't impact hemispheric asymmetry when the mirror was provided at the same time. In addition, the mirror effect can also be found in the alpha SSE results at parietal cortex during preparation phase. The inter-hemisphere activation difference (SSE magnitude) in M^+G^+ was significant lower than in the M^-G^+ condition. This suggested that mirror can attenuate the hemispheric asymmetry when goal information was provided to subjects at the same time. This attenuation may be related to mirror-goal effect.

In summary, the goal effect can be observed in the preparation and execution phases, which goal would increase the desynchronization on the hemisphere ipsilateral to moving hand. Furthermore, the mirror visual feedback (MVF) effect can also be observed in the preparation phase only when the goal was provided. One possible explanation might be the mirror-goal effect.

4.3 Cortical Potential Changes during Movements

EEG topography gives a much more accurate and representative view of the location of cortical alterations. Thus, it should be useful to examine the cortical activity changes during movements. A lot of current dipoles would be summed and formed at around the primary motor cortex during hand movements [36]. This kind of topographic distribution can be observed in all conditions. In addition, Figure 3.9 showed that the fronto-parietal regions were activated to plan the movement after the 'move' cue. Then, the central and frontal regions worked together to execute the movement. But in the two goal conditions,

the parietal cortex was active. Finally, the parietal regions were activated to give internal feedback for improving the performance the next time. This is in line with earlier EEG studies that evaluated the lateralization in the preparatory stage of unilateral hand movement [32].

In addition, the mirror visual feedback (MVF) effect can also be found out in the topographic maps. In the preparation phase, the cortical activity in $M^{-}G^{+}$ condition was more lateralized to the ipsilateral (right) hemisphere comparing to $M^{+}G^{+}$ condition. However, in the no-goal conditions, this phenomenon cannot be observed. The significant difference between these two topographic maps may be related to the mirror-goal effect. During the preparation phase, subjects can get goal information including goal position (20, 40 or 60 degree) and the visual feedback side (mirror or direct). However, for the no-goal movements, subjects only freely move their fingers. This can explain the similar scalp maps in $M^{+}G^{-}$ and $M^{-}G^{-}$ conditions during preparation phase. During movement execution phase, the GFP magnitude of the first peak in $M^{+}G^{+}$ condition is lower than $M^{-}G^{+}$ condition. The reason can be got from the scalp maps which more activity can be observed at left parietal cortex in $M^{-}G^{+}$ condition. In addition, the latency of the first peak in execution phase appeared in $M^{+}G^{+}$ condition was earlier than other conditions. This may be also related to mirror-goal effect.

APPENDIX

MATLAB SOURCE CODE FOR DATA ANALYSIS

The MATLAB codes contain the kinematics, EMG data and EEG data processing and event-related desynchronization (ERD) and sum of square error (SSE) calculation.

```
%% Before ICA

addpath('C:\Users\Administrator\Desktop\Chuang\Mirror_EEG\MATLAB
Code\DATA_Processing_scripts')

Trajectory_explore; % processing Kinematics data
disp('Write down bad trials')
BADtrajectory = input('Bad trials in kinematics: ');

EMG_explore_NEW; % processing EMG data
disp('Write down bad trials')
BADEMG = input('Bad trials in EMG: ');
 save([subject,'_',condition,'_latency.mat'],'latency');

EEG_explore; % processing EEG data
pop_eegplot( EEG, 1, 1, 0);
disp('Write down bad trials')
BADEEG = input('Bad trials in EEG: ');
BADEEG = [BADEEG,121,122,123];
BAD = [BADtrajectory, BADEMG, BADEEG];
save(['Badtrials_',condition,'_',subject,'.mat'],'BAD');
EEG = pop_rejepoch( EEG, BAD);
eeglab redraw

EEG = pop_runica(EEG, 'extended',1,'interupt','on');
ALLEEG = eeg_store(ALLEEG, EEG);


%% During ICA

url = 'http://sccn.ucsd.edu/wiki/Chapter_09:_Decomposing_Data_Using_ICA';
web(url)% open ICA documents in a web


%% After ICA

EEGEMG_synchronize_NEW; % synchronize EEG using EMG
```

```
ERPs_single_condition;%checking ERPs in each condition.

ERPs_explore_NEW; % ERPs comparison among conditions

EMG_compare_plot; % average EMG plot



for j = 1:4 % 4 conditions
   for i = 1:4 % 4 pairs channels (FC3&FC4;C3&C4;CP3&CP4;P3&P4)
      Timefreq_explore; %time-freq  explore
   end
end

Spectra_explore; % power changes explore

PeakVelocity_compare; % peak velocity explore

for i = 1:4 % 4 conditions
   BehaviorError_explore; % movement error explore
end


%% Grand average ERPs & ERSD

Conditions_shift_zero; %shift all conditions' move onset to 0ms which is easy to do the
grand average

Grand_average_ERPs;

Grand_average_ERSD;

SSE_Control_FP12; % SSE of control sites
SSE_beta_C34;% SSE of motor cortex
SSE_alpha_P34;% SSE of parietal cortex


Grand_average_SSE; % plot SSE
```

REFERENCES

1. Ramachandran, V. S., & Altschuler, E. L. (2009). The use of visual feedback, in particular mirror visual feedback, in restoring brain function. Brain, awp135.

2. Touzalin-Chretien, Pascale, and André Dufour. "Motor cortex activation induced by a mirror: evidence from lateralized readiness potentials." Journal of neurophysiology 100.1 (2008): 19-23.

3. Sato, K., Fukumori, S., Matsusaki, T., Maruo, T., Ishikawa, S., Nishie, H. ... & Morita, K. (2010). Nonimmersive Virtual Reality Mirror Visual Feedback Therapy and Its Application for the Treatment of Complex Regional Pain Syndrome: An Open Label Pilot Study. Pain medicine, 11(4), 622-629.

4. Matthys K, Smits M, Van der Geest JN, Van der Lugt A, Seurinck R, Stam HJ, et al. Mirror-induced visual illusion of hand movements: a functional magnetic resonance imaging study. Arch Phys Med Rehabil. 2009; 90: 675–81.

5. Funase K, Tabira T, Higashi T, Liang N, Kasai T. Increased corticospinal excitability during direct observation of self-movement and indirect observation with a mirror box. Neurosci Lett. 2007; 419: 108–12.

6. Garry,M., Loftus,A., Summers,J., 2005. Mirror, mirror on the wall: viewing a mirror reflection of unilateral hand movements facilitates ipsilateral M1 excitability. Exp. BrainRes..163,118–122.

7. Niedermeyer, E., & da Silva, F. L. (Eds.). (2005). Electroencephalography: basic principles, clinical applications, and related fields. Lippincott Williams & Wilkins.

8. Hämäläinen, M., Hari, R., Ilmoniemi, R. J., Knuutila, J., & Lounasmaa, O. V. (1993). Magnetoencephalography—theory, instrumentation, and applications to noninvasive studies of the working human brain. Reviews of modern Physics, 65(2), 413.

9. Onton, J., & Makeig, S. (2009). High-frequency broadband modulations of electroencephalographic spectra. Frontiers in human neuroscience, 3.

10. Pfurtscheller, G., & Da Silva, F. L. (1999). Event-related EEG/MEG synchronization and desynchronization: basic principles. Clinical neurophysiology, 110(11), 1842-1857.

11. Deuschl, G., & Eisen, A. (1999). Recommendations for the practice of clinical neurophysiology (guidelines of the international federation of clinical neurophysiology). Electroencephalography and clinical neurophysiology. Supplement.

12. Cassim, F., Szurhaj, W., Sediri, H., Devos, D., Bourriez, J. L., Poirot, I., ... & Guieu, J. D. (2000). Brief and sustained movements: differences in event-related (de) synchronization (ERD/ERS) patterns. Clinical neurophysiology, 111(11), 2032-2039.

13. Fumuro, T., Matsuhashi, M., Miyazaki, T., Inouchi, M., Hitomi, T., Matsumoto, R., ... & Ikeda, A. (2015). Alpha-band desynchronization in human parietal area during reach planning. Clinical Neurophysiology, 126(4), 756-762.

14. Pfurtscheller, G., & da Silva, F. L. (1999). Functional meaning of event-related desynchronization (ERD) end synchronization (ERS).

15. Frenkel-Toledo, S., Bentin, S., Perry, A., Liebermann, D. G., & Soroker, N. (2013). Dynamics of the EEG power in the frequency and spatial domains during observation and execution of manual movements. Brain research, 1509, 43-57.

16. Meirovitch, Y., Harris, H., Dayan, E., Arieli, A., & Flash, T. (2015). Alpha and Beta Band Event-Related Desynchronization Reflects Kinematic Regularities. The Journal of Neuroscience, 35(4), 1627-1637.

17. Teplan, M. (2002). Fundamentals of EEG measurement. Measurement science review, 2(2), 1-11.

18. Chen, H. L., Lin, K. C., Liing, R. J., Wu, C. Y., & Chen, C. L. (2015). Kinematic measures of Arm-trunk movements during unilateral and bilateral reaching predict clinically important change in perceived arm use in daily activities after intensive stroke rehabilitation. Journal of neuroengineering and rehabilitation, 12(1), 84.

19. Di Fabio, R. P. (1987). Reliability of computerized surface electromyography for determining the onset of muscle activity. Physical Therapy, 67(1), 43-48.

20. Makeig, S., & Onton, J. (2009). ERP features and EEG dynamics: an ICA perspective. Oxford Handbook of Event-Related Potential Components. New York, NY: Oxford.

21. Rejer, I., & Górski, P. (2013). Independent Component Analysis for EEG data preprocessing-algorithms comparison. In Computer Information Systems and Industrial Management (pp. 108-119). Springer Berlin Heidelberg.

22. Makeig, S., Bell, A. J., Jung, T. P., & Sejnowski, T. J. (1996). Independent component analysis of electroencephalographic data. Advances in neural information processing systems, 145-151.

23. Linsker, R. (1988). Self-organization in a perceptual network. Computer, 21(3), 105-117.

24. Delorme, A., & Makeig, S. (2004). EEGLAB: an open source toolbox for analysis of single-trial EEG dynamics including independent component analysis. Journal of neuroscience methods, 134(1), 9-21.

25. Goncharova, I. I., McFarland, D. J., Vaughan, T. M., & Wolpaw, J. R. (2003). EMG contamination of EEG: spectral and topographical characteristics. Clinical Neurophysiology, 114(9), 1580-1593.

26. Ward Jr, J. H. (1963). Hierarchical grouping to optimize an objective function. Journal of the American statistical association, 58(301), 236-244.

27. D. Lehmann and W. Skrandies, "Reference-free identification of components of checkerboard-evoked multichannel potential fields," Electroencephalography and Clinical Neurophysiology, vol. 48, no. 6, pp. 609–621, 1980.

28. Skrandies, W. (2007). The effect of stimulation frequency and retinal stimulus location on visual evoked potential topography. Brain topography, 20(1), 15-20.

29. Koenig, T., & Melie-García, L. (2010). A method to determine the presence of averaged event-related fields using randomization tests. Brain topography, 23(3), 233-242.

30. Bartur, G., Pratt, H., Dickstein, R., Frenkel-Toledo, S., Geva, A., & Soroker, N. (2015). Electrophysiological manifestations of mirror visual feedback during manual movement. *Brain research*, *1606*, 113-124.

31. Laeppchen, C. H., Ringer, T., Blessin, J., Seidel, G., Grieshammer, S., Lange, R., & Hamzei, F. (2012). Optical illusion alters M1 excitability after mirror therapy: a TMS study. Journal of neurophysiology, 108(10), 2857-2861.

32. Meng, L. F., Lu, C. P., & Li, Y. W. (2008). Hemispheric lateralization of event-related brain potentials in different processing phases during unimanual finger movements. Sensors, 8(4), 2900-2912.

33. Avanzini, P., Fabbri-Destro, M., Dalla Volta, R., Daprati, E., Rizzolatti, G., & Cantalupo, G. (2012). The dynamics of sensorimotor cortical oscillations during the observation of hand movements: an EEG study. *PLoS One*, *7*(5), e37534.

34. Deconinck, F. J., Smorenburg, A. R., Benham, A., Ledebt, A., Feltham, M. G., & Savelsbergh, G. J. (2014). Reflections on Mirror Therapy A Systematic Review of the Effect of Mirror Visual Feedback on the Brain. Neurorehabilitation and neural repair, 1545968314546134.

35. Marois, R. (2002). The cortical basis of motor planning: does it take two to tango? Nature neuroscience, 5(12), 1254-1255.

36. Praamstra P, Torney L, Rawle CJ, Chris Miall R. Misconceptions about mirror-induced motor cortex activation. Cereb Cortex. 2011; 21:1935-1940.

37. Koski, L., Wohlschläger, A., Bekkering, H., Woods, R. P., Dubeau, M. C., Mazziotta, J. C., & Iacoboni, M. (2002). Modulation of motor and premotor activity during imitation of goal-directed actions. Cerebral cortex, 12(8), 847-855.

38. Nojima, I., Mima, T., Koganemaru, S., Thabit, M. N., Fukuyama, H., & Kawamata, T. (2012). Human motor plasticity induced by mirror visual feedback. The Journal of Neuroscience, 32(4), 1293-1300.